uOttawa

L'Université canadienne
Canada's university

FACULTÉ DES ÉTUDES SUPÉRIEURES ET POSTOCTORALES

uOttawa

L'Université canadienne
Canada's university

FACULTY OF GRADUATE AND POSDOCTORAL STUDIES

Jeffery Bond
AUTEUR DE LA THÈSE / AUTHOR OF THESIS

M.Sc. (Physics)
GRADE / DEGREE

Department of Physics
FACULTÉ, ÉCOLE, DÉPARTEMENT / FACULTY, SCHOOL, DEPARTMENT

The Optimization of Carbon Nanotube Growth Parameters for Photonics

TITRE DE LA THÈSE / TITLE OF THESIS

Dr. P. Finnie
DIRECTEUR (DIRECTRICE) DE LA THÈSE / THESIS SUPERVISOR

CO-DIRECTEUR (CO-DIRECTRICE) DE LA THÈSE / THESIS CO-SUPERVISOR

EXAMINATEURS (EXAMINATRICES) DE LA THÈSE / THESIS EXAMINERS

Dr. R. Bhardwaj

Dr. B. Campbell

Dr. H. Schriemer

Gary W. Slater
Le Doyen de la Faculté des études supérieures et postdoctorales / Dean of the Faculty of Graduate and Postdoctoral Studies

The optimization of carbon nanotube growth parameters for photonics

Jeffery Bond

Thesis submitted to the
Faculty of Graduate and Postdoctoral Studies
In partial fulfillment of the requirements
For the Master of Science degree in physics

Department of Physics
University of Ottawa

Your file Votre référence
ISBN: 978-0-494-32439-4
Our file Notre référence
ISBN: 978-0-494-32439-4

Abstract

Suspended carbon nanotubes are of particular interest for optical and optoelectronic applications because of their superior optical properties. The purpose of this work is to explore sample preparation and chemical vapour deposition (CVD) process parameters to develop methods of fabricating large quantities of freely suspended single walled carbon nanotubes (SWNTs). Parameters including CVD hydrogen soak temperature, growth temperature, choice of catalyst, gas flow rate, and gas composition were examined.

Various techniques were tested for their practical capability to suspend SWNTs. A simple procedure was used to suspend SWNTs over networks of randomly organized thick MWNTs on unpatterened substrates. In a more versatile procedure SWNTs were suspended between adjacent pillars of vertically aligned MWNT forests on patterned substrates. Large quantities of SWNTs were also suspended over pre-fabricated trenches in the substrate. All of these laterally suspended SWNT were found to be useful for optical studies.

Acknowledgements

I would like to thank everyone who assisted in this work. My supervisor, Paul Finnie, was always willing to discuss results and offer suggestions. Many IMS staff members offered assistance including Jacques Lefebvre, Kate Kaminska, Paul Marshall, Guy Austing, Martha Tomlinson, Jeff Fraser, Simona Moisa, Hue Tran, Philip-Chow Chong and Terry Quance.

Table of Contents

Table of Figures

1 Introduction

1.1 Carbon nanotubes

Since their discovery [1], carbon nanotubes (CNT) have shown great potential in a variety of areas. CNTs have excellent mechanical and electrical properties. The Young's modulus of CNTs is very high [2]. The electrical properties of CNTs have been shown to exhibit either semiconducting or metallic properties. Metallic nanotubes have applications as conducting wires [3, 4]. Semiconducting nanotubes can be used as field effect transistors [5, 6]. Combinations of nanotubes can be used to produce rectifiers [7, 8] and other multi-terminal devices [9].

CNTs have many similarities to graphite. Graphene is a sp^2-hybridization of carbon atoms arranged in a hexagonal lattice. A graphene sheet rolled up to form a cylinder is referred to as a single walled carbon nanotube (SWNT). The electrical properties of CNTs depend on the arrangement of atoms in the nanotube. The structure of a SWNT is commonly defined by a vector on a graphene sheet. This vector indicates how the sheet could be rolled up to form the particular type of nanotube. The rollup vector or chiral vector traces the circumference of the nanotube. Defining the chiral vector (**b**) in terms of the lattice base vectors $\mathbf{a}_1$ and $\mathbf{a}_2$ ($\mathbf{b} = n\cdot\mathbf{a}_1 + m\cdot\mathbf{a}_2$) allows for comparison of different chiral vectors. Nanotubes are commonly referred to using n and m indices written in the form (n, m). In this case (figure 1) the type or chirality of the nanotube indicated is a (6, 6) nanotube ($\mathbf{b} = 6\cdot\mathbf{a}_1 + 6\cdot\mathbf{a}_2$). If the indices are equal the nanotube is referred to as armchair. If one of the indices is zero, then the nanotube is referred to as zigzag. Otherwise the nanotube is simply called chiral. These terms refer to how the atoms are arranged along the chiral vector. The optical and electrical properties of a

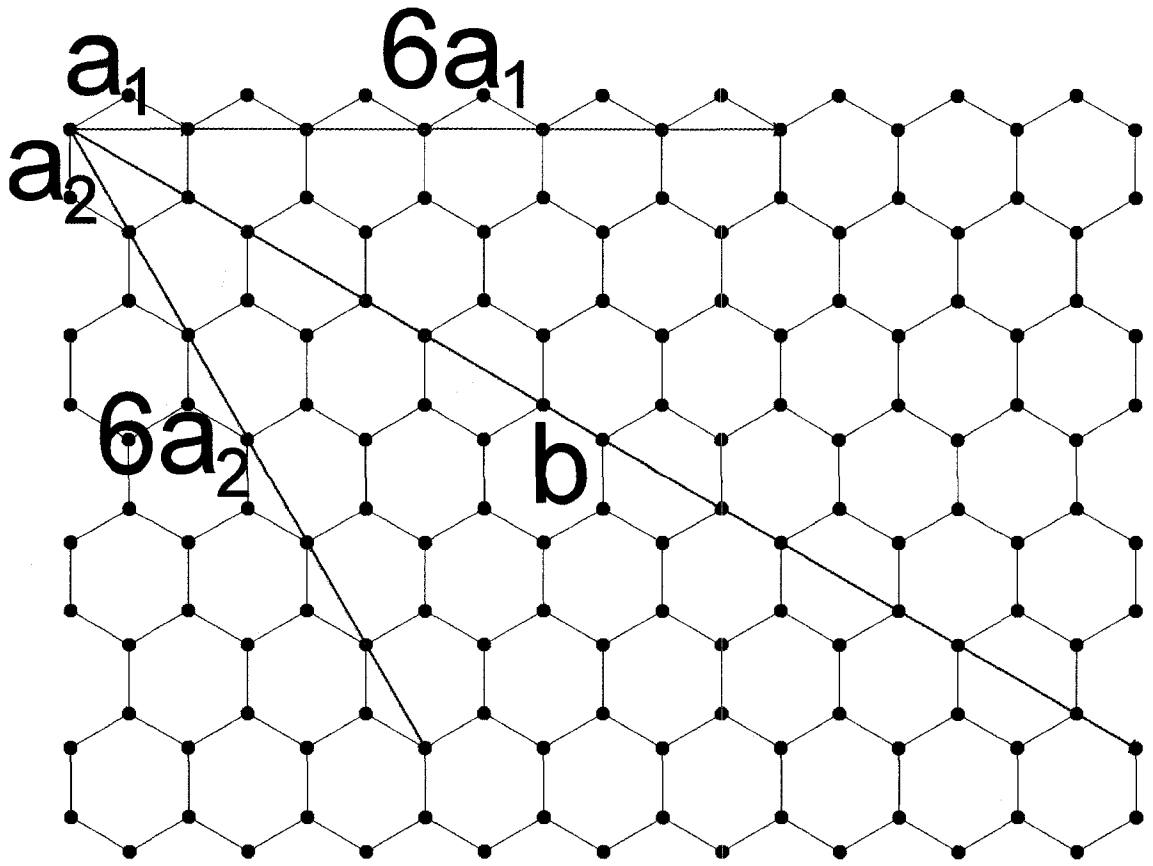

Figure 1 Chiral vectors depicted on a graphene sheet. The lattice vectors are chosen to be $\mathbf{a}_1$ and $\mathbf{a}_2$. A (6, 6) armchair nanotube is depicted by the rollup or chiral vector **b**.

nanotube depend on the modulus of the indices. A nanotube has metallic conduction properties when the difference between the indices is an integer multiple of three ($n - m = 3i$, where i is an integer) [10]. All other SWNT behave like semiconductors.

In contrast to a SWNT, another type of nanotube is called a multiwalled nanotube (MWNT). This type of nanotube has more than one atomic layer of carbon. It can be pictured as a series of nanotubes with different diameters all sharing the same central axis (figure 2b).

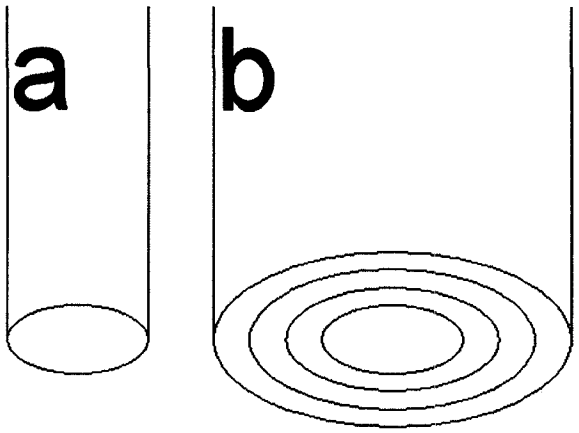

Figure 2 Comparison of single walled and multiwalled carbon nanotubes. A single walled carbon nanotube is depicted with one atomic layer of carbon in (a) and a multiwalled carbon nanotube is depicted with numerous atomic layers of carbon in (b).

There are differences in the properties of SWNT and MWNT. Most notable, the outer diameter of MWNTs is generally larger than that of SWNTs. The diameter of a SWNT is typically on the order of a nanometre however diameters have been reported as small as 0.4 nm [11]. Lengths of SWNTs in our work are typically on the order of tens of microns however SWNTs with lengths of 4 centimetres have been reported [12]. In contrast the diameter of a MWNT is typically on the order of tens of nanometres. There are also differences in the optical properties of SWNT and MWNT. Radial breathing modes (section 2.3) and photoluminescence (section 2.4) have been detected from SWNTs but not thick MWNTs. These properties are detailed further in later sections.

1.2 Chemical vapour deposition

There are a variety of methods by which CNTs have been produced. These methods include arc-discharge [1, 13, 14], laser ablation [15, 16], pyrolysis [17, 18] and chemical vapour deposition (CVD) [19, 20, 21, 22]. In particular, CVD shows great promise for

producing large quantities of high quality carbon nanotubes at relatively low cost [23]. As such, all of the carbon nanotubes examined in this work were grown using CVD.

Generally, SWNT CVD involves heating metal catalyst particles to a high temperature in the presence of a carbon-containing gas. The key process parameters of CVD are the growth temperature [24, 25, 26, 27], the catalyst [28, 29, 30] and the carbon-containing gas [31]. Typical growth temperatures range from 500-1000°C, however nanotubes have been reported to grow at temperatures as low as 350°C [32]. Transition metals, including iron, cobalt and nickel, are commonly used as catalysts, however a large selection of metals have been used to produce CNTs [33]. A variety of different carbon source gasses have been used including methane [20], ethanol [34], carbon monoxide [35], ethylene [36] and acetylene [37].

Growth of CNTs involves the dissociation of carbon-containing gas by the metal catalyst. Dissociated carbon atoms then saturate the catalyst. A rational for choosing transition metals such as iron, cobalt, and nickel lies in the phase properties of these materials [23]. At nanotube growth temperatures, carbon has a finite solubility in these metals. Qualitatively, the source gas supersaturates the metal catalyst with carbon. The precipitation of carbon from the catalyst results in the formation of nanotubes. The tubular arrangements with sp^2 bonds is the favoured low energy structure as there are no dangling bonds present in other structures such as graphite [38]. Effectively, the source gas drives the formation of a nanotube from the metal catalyst.

There are two different growth modes responsible for nanotube growth using CVD [39, 40]. Base growth occurs when the catalyst remains fixed with respect to the substrate and the nanotube grows away from the catalyst particle (figure 3a). Tip growth

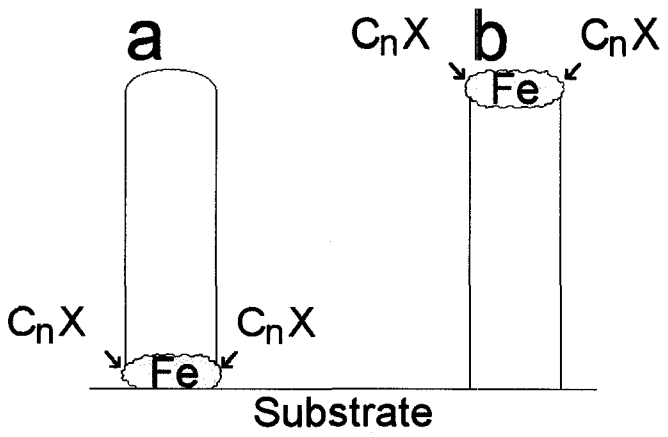

Figure 3 Comparison of base and tip growth. Base growth is shown in (a). The nanotube moves away from the fixed catalyst with growth. Tip growth is shown in (b). The catalyst moves away from the nanotube with growth.

occurs when the grown nanotube remains fixed with respect to the substrate and the catalyst particle moves during growth (figure 3b).

The key difference between the two growth modes is the adhesion between the catalyst, the nanotube and the substrate. Here adhesion refers to the ability of the area of contact between two dissimilar bodies to resist mechanical separation [41]. In base growth, the adhesion between the catalyst and the substrate is higher than the adhesion between the nanotube and the substrate. Movement of the nanotube requires less energy than movement of the catalyst. In tip growth, the adhesion between the nanotube and the substrate is higher than the adhesion between the catalyst and the substrate. Less energy is required to move the catalyst than the nanotube. In figure 3 the nanotubes are shown growing perpendicular to the substrate however a specific nanotube orientation is not required for a particular type of growth mode.

1.3 Catalyst

Growth of nanotubes initiates from the metal catalyst. Because of this, many of the properties of a nanotube can be traced back to properties of the catalyst during the nanotube's growth. Variations in nanoparticle properties including size, composition and adhesion to the substrate can have large effects on the properties of grown nanotubes. Certain catalyst properties including morphology and composition have also been shown to change at elevated temperatures [30, 42]. For example, the catalyst film has been shown to break up into nanoparticles when heated to nanotube growth temperatures [43]. The diameter of these nanoparticles depends on a number of variables including temperature and initial catalyst film thickness [44]. Growth temperature, catalyst composition and catalyst thickness are important parameters in nanotube growth.

1.4 Suspending nanotubes

This work is primarily concerned with fabricating SWNTs with good optical [45] properties. These properties can be strongly influenced depending on whether the segment of nanotube is freely suspended or not. Here, "freely suspended" refers to a segment of nanotube which is isolated and not making contact with any surface. These segments are in contact only with the ambient atmosphere. Freely suspended nanotubes have certain optical properties which are superior to surface nanotubes. For example, experimentally it has been shown that photoluminescence [45] from suspended nanotubes has a high quantum efficiency [46], and the electroluminescence [47] from suspended nanotubes is stronger than nanotubes on the substrate. Suspended SWNTs also have very good electronic [48], optoelectronic [49], and phonon-related [50, 51, 52] properties.

Utilization of these improved optical properties requires reliable techniques of producing freely suspended nanotube segments.

In early work on SWNT chemical vapour deposition (CVD), nanotubes were suspended from lithographically defined pillars [53]. Suspended nanotubes have since been fabricated by growing on other lithographically textured [54] and even holey [55] substrates. Nanotubes have been suspended fortuitously by growing over particles on the surface, either deposited [19], or self-organized by Si-crystal agglomeration [56]. Nanotubes deposited on a surface have been suspended by etching the substrate away beneath the nanotubes [57].

1.5 This work

Efforts are made to produce high yields of freely suspended SWNT since their optical properties show great potential. Specifically attempts were made to increase nanotube yield, increase SWNT concentration and suspend nanotubes. A study of the effects of adjustments to various CVD process parameters was conducted. Hydrogen soak temperature, growth temperature, ethanol concentration, catalyst type, catalyst thickness, gas flow rate, and gas composition were found to be key variables in controlling the nanotubes produced.

Scanning electron microscopy (SEM) was used for rough characterization. Nanotube position, length and a general indication of the nanotube diameter could be readily identified through SEM. Atomic force microscopy (AFM) proved to be useful in identifying the diameters of isolated nanotubes. Raman spectroscopy was used primarily to identify relative concentrations of SWNTs on samples and discover variations in nanotube diameter between samples. Some indication of nanotube quality was also

determined using Raman spectroscopy. Photoluminescence (PL) spectroscopy and imaging were used to identify freely suspended thin semiconducting nanotubes.

A variety of techniques were found to be useful for producing freely suspended SWNTs. A straightforward method is to suspend SWNTs from MWNTs. Unpatterened substrates were used to grow a random network of thick MWNTs. SWNTs were then grown overtop of the MWNTs resulting is suspended segments of SWNT which bridge the MWNTs. A more flexible technique allowing for control over the position of the suspended nanotubes was found. Patterned substrates with vertically aligned MWNT pillars were utilized to suspend segments of SWNTs. Pre-fabricated trenches etched into the substrate were also used to suspend large numbers of SWNTs. Freely suspended nanotubes were produced by all of these methods.

2 Characterization

Various techniques including scanning electron microscopy (SEM), atomic force microscopy (AFM), Raman spectroscopy, photoluminescence (PL) spectroscopy, and PL imaging were used to characterize the grown product. Each method reveals different information about the grown product. SEM allows for rapid examination of nanotube location and orientation. AFM can reveal the diameter of isolated nanotubes. Raman spectroscopy can be used to determine the relative concentrations of SWNT and nanotube quality. Photoluminescence allows for direct measurement of nanotubes' optical bandgap.

2.1 Scanning electron microscopy

Scanning electron microscopy (SEM) is a powerful technique for imaging CNTs. There are two modes that can be utilized to image nanotubes. These modes are imaging through direct geometric contrast and imaging by charging mode [58, 59].

The geometric contrast mode can be used to image nanotubes (figure 6a). These nanotubes or segments of nanotubes can be detected by variations in the backscattered and secondary electron signals as the scanning beam rasters over the nanotube. The diameter of a nanotube imaged using this type of imaging mode can be close to the nanotube's actual diameter depending on the beam conditions.

Imaging through the charging mode relies on differential charging of a conducting nanotube and an insulating substrate [59]. Nanotube segments imaged using this mode must be in direct contact with the substrate and appear as blurred bright lines (figure 6b). A rough explanation of this imaging mode is as follows: SEM imaging with a low accelerating voltage (1 kV) develops a global positive surface charging potential on a

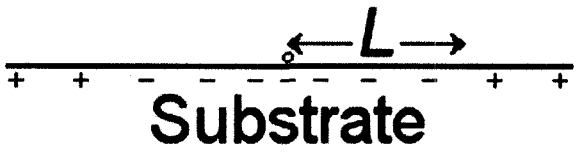

Figure 4 Scanning electron microscopy imaging of nanotubes through charging mode. Electrons diffuse from the nanotube (small circle) into the substrate resulting in a negative charging of the surface within the electron diffusion length (L) of the nanotube. The differences in electrostatic potential of the substrate can be imaged with scanning electron microscopy.

silicon substrate topped with an insulating silicon dioxide layer. Nanotubes develop a negative charge relative to the globally positive silicon dioxide surface potential. Electrons spread from the nanotube into the substrate. This produces a locally negatively charged surface potential spreading the electron diffusion length (L) away from the nanotube (figure 4). The contrast in electrostatic potential between the negatively charged substrate surrounding the nanotube and the positively charged global substrate can be imaged with SEM. This effect is most easily observed from thin nanotubes. Nanotubes whose radius is much less than the charge diffusion length appear to have a radius of the charge diffusion length.

Both the geometric contrast and the charging modes can be observed in a single image. Comparison of the two modes can indicate if a nanotube is suspended or on the substrate. Neither mode requires the use of conductive coatings to enhance the images. SEM is capable of quickly imaging the location of carbon nanotubes [58]. Because it is such a powerful tool, a large portion of the characterization of nanotubes was performed using SEM. An accelerating voltage of 1 kV was most commonly used as this voltage has been shown to have the highest image contrast for charging mode [58].

Generally, there were two different views used to image nanotubes. These views are plan view and side view. Figure 5 shows the location of the sample with respect to the SEM column and detector.

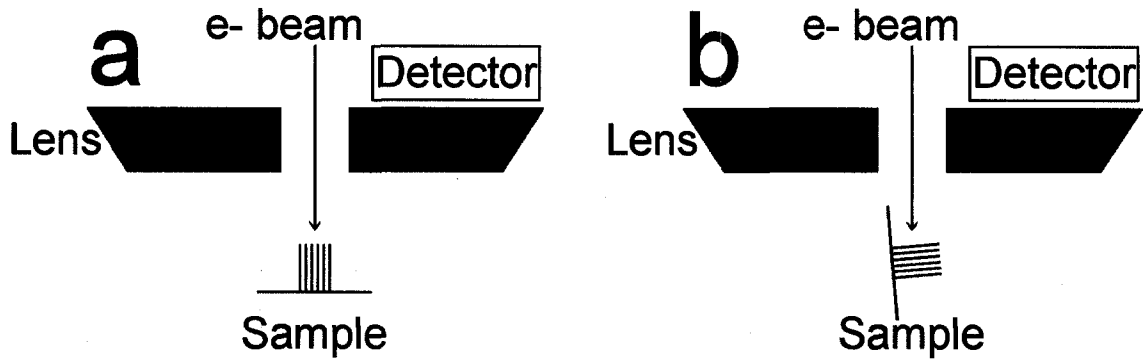

Figure 5 Schematic view of a sample in a scanning electron microscope. The sample is mounted in plan view (a) and in side view (b). These images are not to scale.

2.1.1 Plan view

Plan view imaging was most commonly used. Generally the depth of the area imaged was much less (<10 μm) than the length and the width (>1 mm) of the samples. As a high resolution is desired and a low depth of field is acceptable, short working distances between the lens and the sample were used varying from between 3.0 and 3.5 mm.

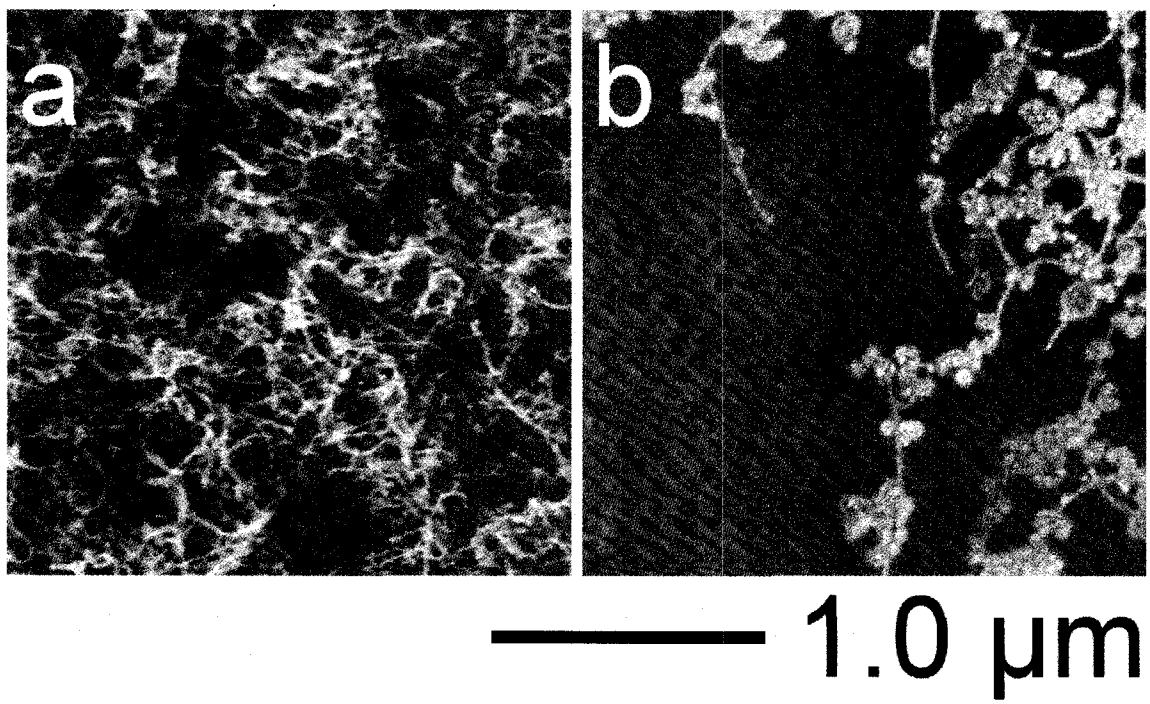

Figure 6 Plan view images of nanotubes. Image (a) contains a forest of thicker multiwalled nanotubes and (b) presents thin likely single walled nanotubes. Both images were taken at 1 kV.

Typical plan view images of nanotubes are shown in figure 6.

2.1.2 Side view

Some growth conditions result in the formation of densely packed nanotubes or forests. Samples with a high concentration of nanotubes primarily orientated normal to the substrate are referred to as vertically aligned forests. The edges of nanotube forest samples revealed information about nanotube length and alignment. Samples were held with the normal to the substrate at an angle of 85° to the electron beam. This was done using a support which holds samples at right angles to the SEM stage. The stage was then inclined by 5°. The working distance was set to between 5 and 8 mm. Figure 7 is an example of one of the side view SEM images.

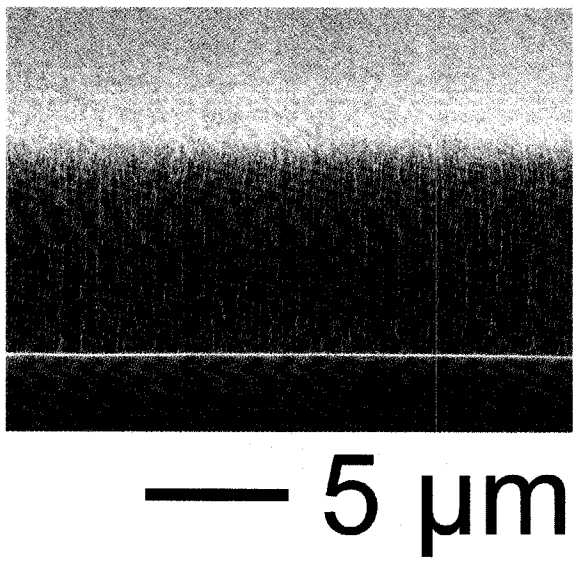

Figure 7 Side view of nanotube forest. Aligned nanotubes, all of roughly the same length, are standing up parallel to the normal of the substrate. Silicon dioxide can be seen at the bottom of the image. The top of the image shows the top of the forest eventually fading out past the depth of field of the microscope.

2.1.3 Scanning electron microscope deposition

SEM has been shown to damage CNTs [60, 61]. It is also known to cause electron beam induced carbon deposition [62, 46]. Over time it was noticed that material was deposited on the exterior of nanotubes, altering their properties. An area of nanotubes (figure 8a) was imaged for 15 minutes. During this time some material was deposited on the imaged nanotubes, however the bulk of the deposition occurred just outside of the imaged area (figure 8b). Photoluminescence signals from nanotubes have been noticed to disappear after SEM imaging [46]. Nanotube damage and carbon coatings cause the reduction in these signals but the mechanism is not yet entirely clear.

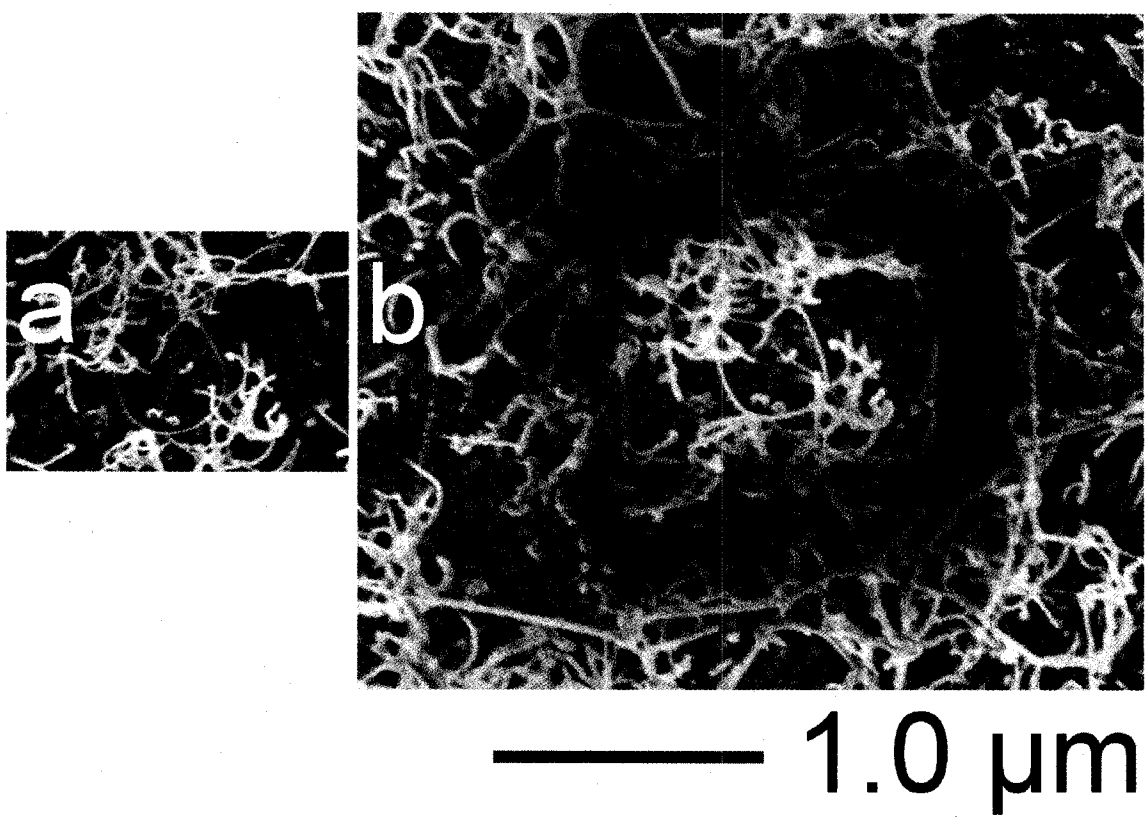

Figure 8 Scanning electron microscopy deposition. Image (a) shows the initial appearance of some nanotubes. These nanotubes were imaged for 15 minutes. The magnification of the microscope was decreased and image (b) was taken. Some material built up on the imaged nanotubes however the largest amount of deposition occurred just outside the imaged area.

2.1.4 Imaging long nanotubes

The SEM signal from some long nanotubes is not strong enough to facilitate imaging the whole nanotube at once using a low magnification. Figure 9 presents an area where a 1 mm nanotube is known to exist however its SEM signal is not strong enough to view at this magnification. A trick can be used to indicate the location and approximate length of this nanotube. Charge accumulates in silicon dioxide when it is imaged using SEM [63]. Some of this accumulated charge dissipates over time. A pattern was traced out in the silicon dioxide at high a magnification and then the SEM was quickly switched to a low

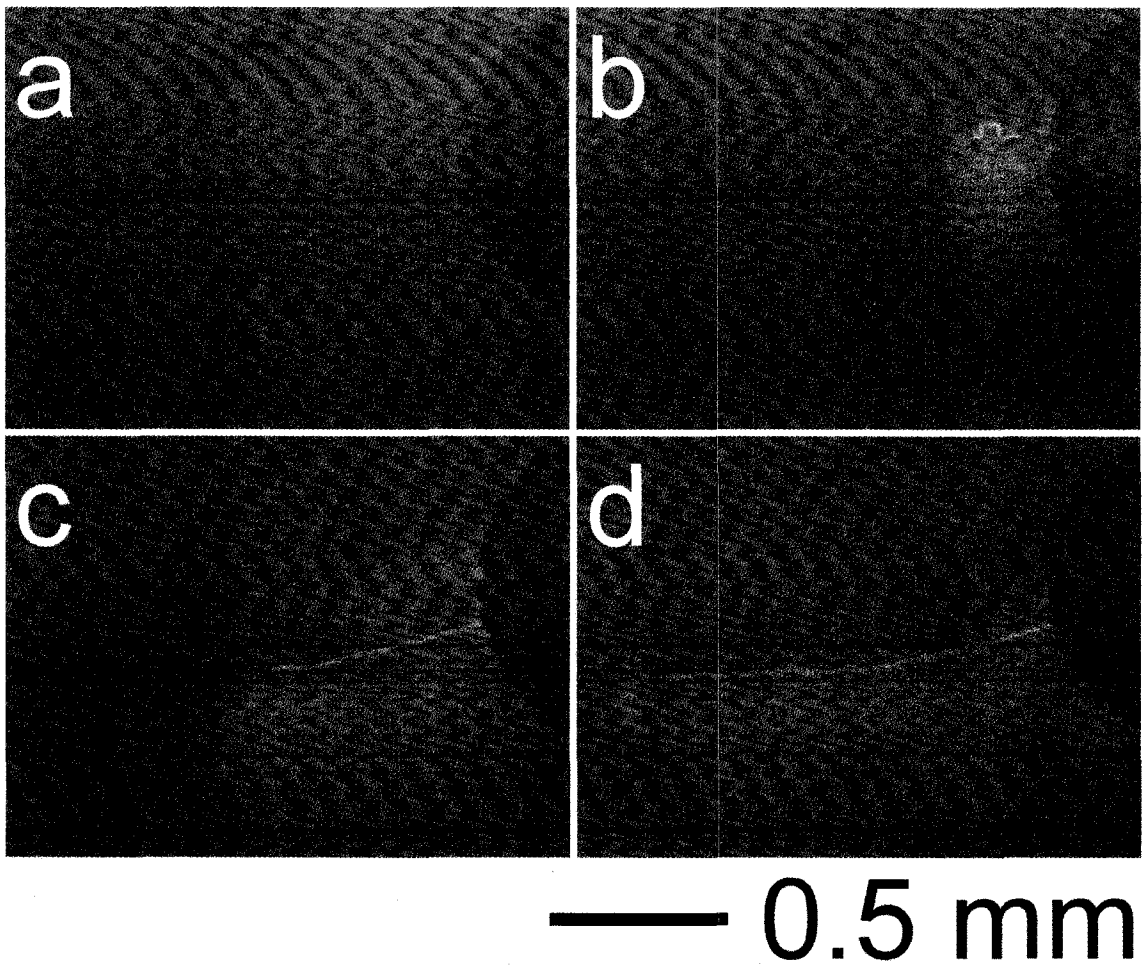

Figure 9 Imaging of charged silicon dioxide. Patterns can be traced into the silicon dioxide by imaging with high magnification and then viewed with low magnification. A nanotube was traced out in (d). All of the images are of the same area.

magnification before an image was taken (figure 9b). Presumably, the negative charges accumulated in the area imaged at high magnification are visible in low magnification. This effect is short lived and so is a result of charge accumulation as oppose to some from electron beam induced deposition. This effect can be used to trace out and indicate the position of nanotubes. Starting where the nanotube met the catalyst a length of the nanotube was scanned at a magnification of 20K times and at accelerating voltage of 1 kV. When the end of the nanotube was reached, the magnification was quickly switched to 50 times and the image in figure 9d was taken. In figure 9c, the whole length of the nanotube was not traced out. Figure 9a shows the uncharged region.

SEM cannot be used for direct measurement of the diameter of thin nanotubes [59]. Differential charging artificially magnifies the diameter of the nanotubes viewed in images. SEM reveals the presence of a nanotube, however some other technique is required for measuring the diameter of nanotubes.

2.2 Atomic force microscopy

Tapping mode atomic force microscopy (AFM) is a tool which can be used to image nanotubes. Subject to some assumptions, AFM allows for the measurement of nanotube diameter. Assuming that the nanotube is isolated (not in a bundle), it has a cylindrical shape and is not compressible, the actual diameter of the nanotube can be experimentally determined by measuring the maximum elevation of the nanotube relative to the local elevation of the substrate. The width of a nanotube as observed in an AFM image is the convolution of the actual nanotube diameter and the radius of curvature of the AFM tip. AFM is however more time consuming and more complicated than SEM. It is very sensitive to surface roughness and surface contamination. Because AFM is generally

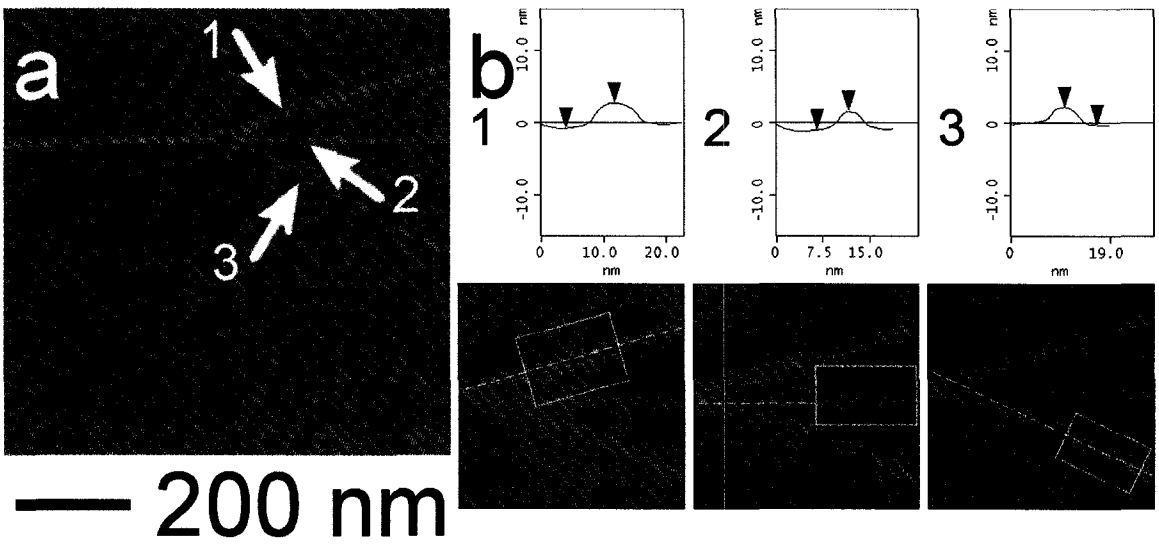

Figure 10 Atomic force microscopy of a bundling nanotube. Part (a) depicts the surface height in an area while part (b) shows how the nanotube diameters were measured at the various locations. Nanotube diameter was taken to be the change in elevation between the red arrows.

slow and is only suited for the observation of surface features, we made a limited use of AFM.

Some nanotube characterization was performed using AFM. Difficulty was found in imaging the nanotube forests. The flexibility in the forests allowed for movement in the nanotubes as the tip passed over resulting in dissimilar trace and retrace curves. AFM images isolated nanotubes lying flat on the substrate well. The following is an example of such an image. The diameters of the nanotubes at the arrows were measured. The nanotube heights at (1), (2), and (3) are 3.5 nm, 2.5nm, and 2.5 nm respectively. The dots covering the substrate are the catalyst nanoparticles.

Neither SEM [63, 64] nor AFM [65] is capable of determining the electrical properties of nanotubes without the preparation of special devices.

2.3 Raman spectroscopy

Raman spectroscopy can be used to estimate diameters of SWNT as well as the quality of nanotubes [66, 67]. This spectroscopy technique examines the low frequency vibrational and rotational modes in a system of atoms. A schematic diagram of one of our Raman experiments is shown in figure 11. A laser is used to produce monochromatic light. A lens focuses the laser light on a nanotube sample. Some of the photons are inelastically scattered by phonons within the nanotube system. Some of the scattered photons travel back through the lens and are reflected off of a beam splitter. Elastically scattered photons of the incident laser energy are blocked using a notch filter. The inelastically scattered light is then focused by another lens into a spectrometer.

Detecting and plotting the intensity distribution of the inelastically scattered photons with their corresponding energy displacement yields the Raman spectra. A typical Raman spectra for nanotubes grown at 850°C is shown in figure 12. The excitation was performed in air using a 632.8 nm HeNe laser. The energy shifts between the incident and the scattered photons reveal information about the phonon modes of the nanotubes which are excitable by the HeNe laser.

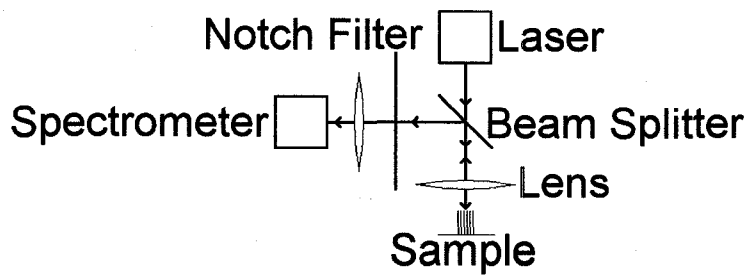

Figure 11 Schematic of Raman spectroscopy setup.

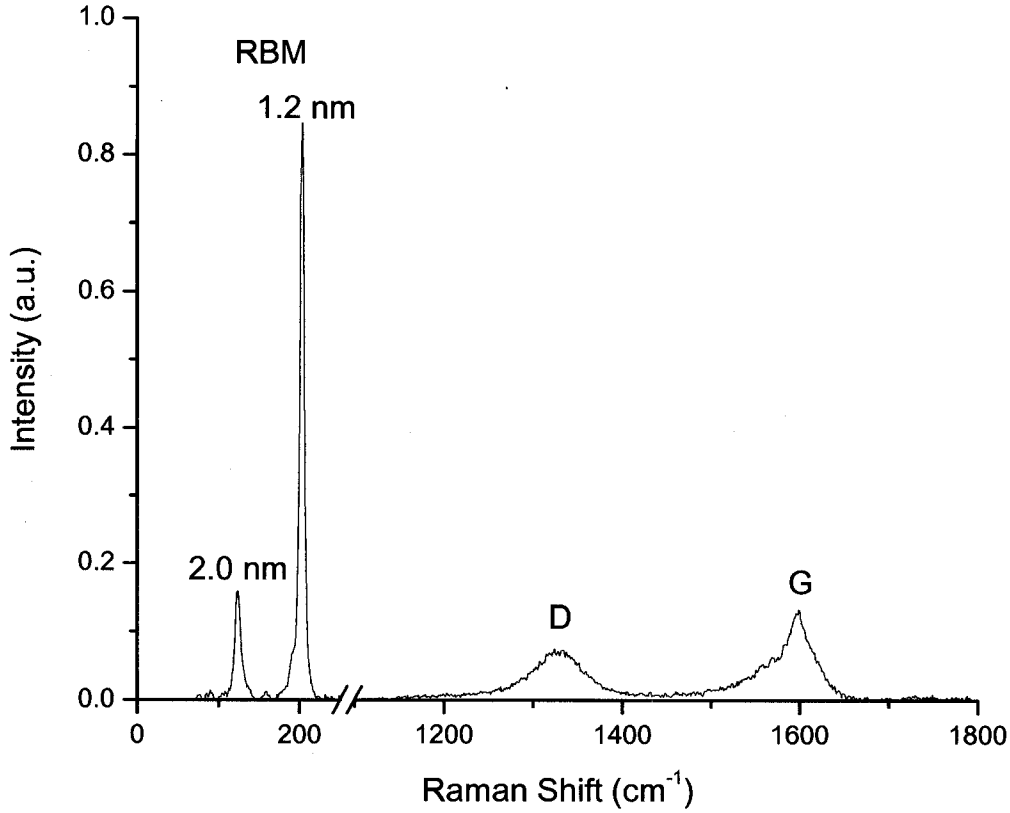

Figure 12 Typical Raman spectra for a sample grown at 850°C. A HeNe laser was used to illuminate a roughly 1 μm diameter spot.

Several Raman peaks have been shown to be of particular interest in the analysis of carbon nanotubes [68]. These peaks include the G band, the D band and the radial breathing mode (RBM). The G and the D bands result from the sp^2 bonds and so are present in all graphitic like carbon structures including both SWNT and MWNT. The G band refers to the peak in the range of 1550-1605 cm^{-1}. The 'G' refers to graphite. The D band is the peak around 1350 cm^{-1}. This band is related to disorder. A defect in the sp^2 graphitic structure is required to excite the D band vibrational mode. Defective nanotubes will produce a high D band peak however a high D band peak is not necessarily caused by defective nanotubes. Amorphous carbon surrounding high quality nanotubes can result

in a high D bank peak. Comparing the ratio of the D and G bands can give an indication of the concentration of defects present in the sample. SWNTs tend to have high G to D ratios, and the detailed structure of the G band may provide evidence for the presence of SWNTs.

The other peak of interest is the RBM. This mode comes from vibrations which cause the radius of the nanotube to oscillate. Van der Waals interactions between CNTs and other molecules tend to distort this radial oscillation. RBMs are strongest in freely suspended SWNT [69]. The RBM signal is reduced by bundling and direct contact with the substrate. RBMs are not found from thick MWNT. The observation of a sharp strong RBM in the band from 100 cm^{-1} to 300 cm^{-1} is evidence of the presence of a SWNT as opposed to a MWNT [68]. By examining the energy shift in the RBM certain properties of a nanotube can be found. Specifically, the diameter of a nanotube is roughly inversely proportional to the RBM frequency (d=2.48·$10^{-5}/\omega$) [68]. The RBM can also reveal certain electrical properties of a nanotube [70].

2.4 Photoluminescence spectroscopy/imaging

Photoluminescence (PL), or fluorescence, is also another powerful technique which can be used to characterize CNTs [45, 46, 71, 72]. PL allows for the direct measurement of a semiconducting nanotube's optical bandgap. The bandgap of a freely suspended nanotube varies depending on a nanotube's chiral vector and typically range from zero for a metallic nanotube to a few electron volts for a narrow semiconducting SWNT [66]. PL begins with the absorption of a photon (figure 13a) to create an electron-hole pair, or exciton (figure 13b). The energy of the absorbed photon must be greater than the bandgap of the nanotube. This energy of the exited exciton decays to the bandgap through phonon

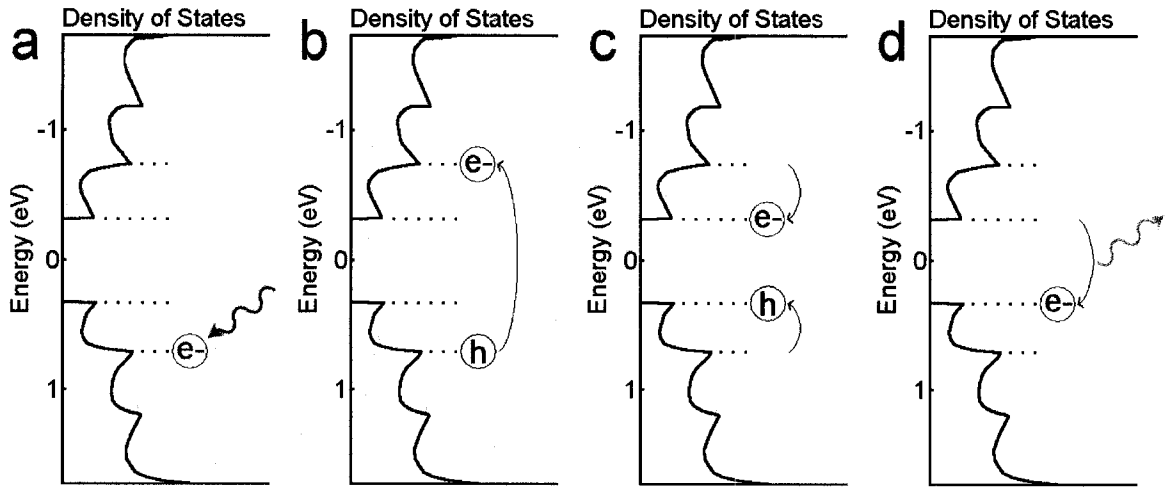

Figure 13 Time sequence of photoluminescence. A photon excites and electron (a) generating an excited exciton (b). The exciton decays to have energy of the bandgap through phonon emission (c). The exciton recombines to produce a characteristic photon (d). The density of states plot was based on a (10, 0) nanotube from [74] with a bandgap of roughly 0.6 eV.

emission (figure 13c). A photon is then emitted by the recombination of the electron-hole pair (figure 13d). One of the key components of PL is that the energy of the emitted photon is different from the absorbed incident photon. The detection of this photon allows for direct measurement of the nanotube's bandgap.

Strong luminescence is evidence that freely suspended SWNT are present [45]. Semiconducting SWNTs are expected to emit PL, however bundles or thick MWNTs are not. Bundling and contact with the surface have been observed to reduce the PL signal [73]. The leading explanation is that bundling and contact with the substrate perturb the density of states broadening the bandgap [74]. Recent reports suggests that PL is possible from double walled nanotubes (DWNTs) [75, 76]. The possibility that some of the nanotubes in this report examined with photoluminescence are DWNT cannot be eliminated. Similarly, although bundling and contact with the substrate tend to quench SWNT PL, the presence of small bundles of nanotubes also cannot be ruled out.

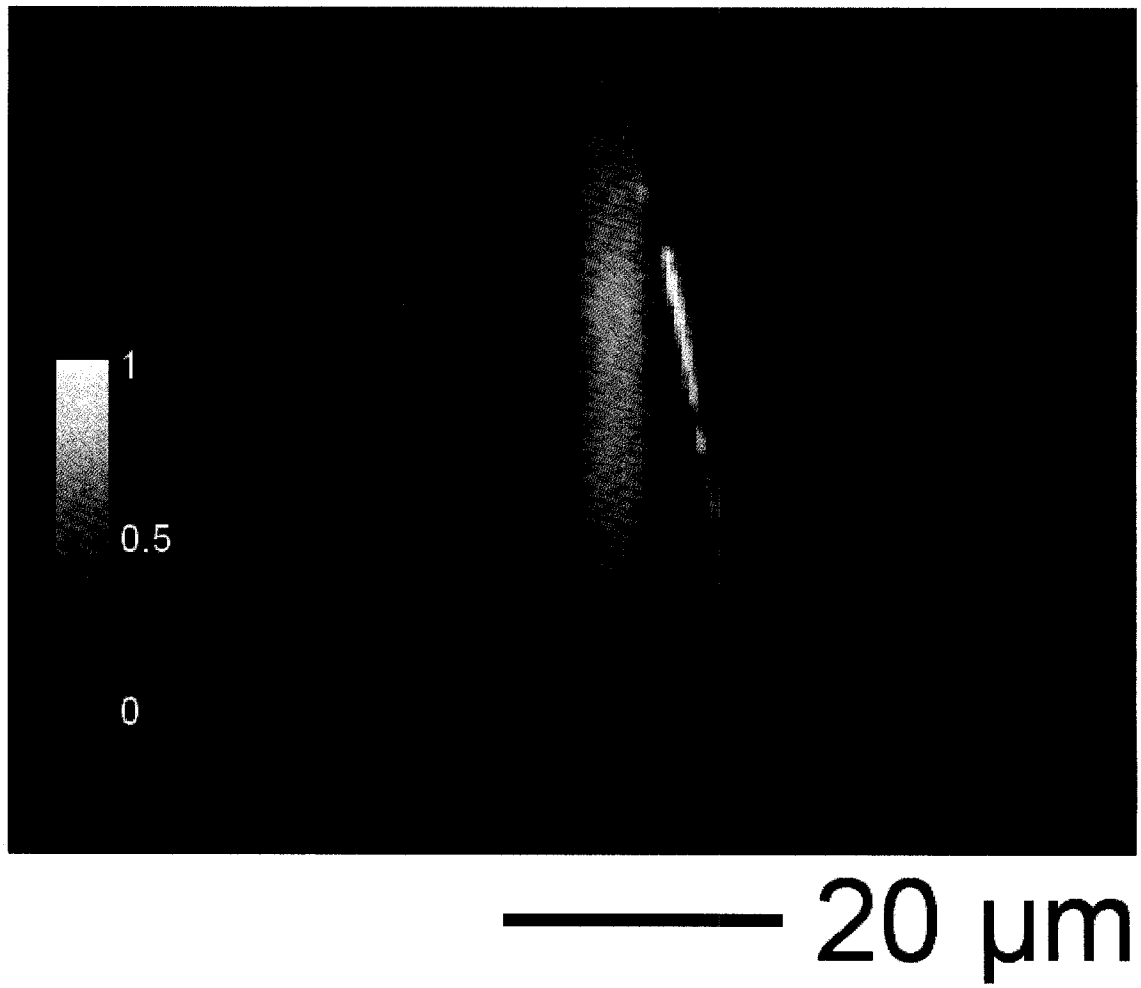

Figure 14 Photoluminescence image of a freely suspended nanotube segment. The photoluminescence is strongest in the region where the nanotube is suspended.

Some of the samples containing CNTs were examined using PL. An elliptical spot with dimensions ~60 μm × ~40 μm from a defocused diode laser beam (860 nm) was used to produce electron-hole pairs (excitons) in the nanotube. The emitted radiation, through recombination at the bandgap, can be found in the infrared for most semiconducting SWNTs. A 2D InGaAs photodiode camera which is sensitive to infrared radiation (~1.0 μm to 1.6 μm) was used to detect the PL signal. Figure 14 is a PL image of a carbon nanotube. The substrate was pre-patterned with lithography to produce trenches. The straight bright line represents a segment of a nanotube which is freely

suspended over one of the trenches. The PL signal is strong from this segment. At the top end of the bright section, the nanotube is not easily visible. Here the nanotube is in contact with the surface and the PL signal is quenched.

3 CVD Synthesis

In order to optimize the growth process to reach our goal, an understanding of how different process parameters influence the growth and final product must be attained. The key process parameters to CVD are growth temperature, catalyst, and carbon source gas. Experiments were performed testing how grown nanotubes vary under different growth temperatures and different hydrogen soak temperatures. A variety of different catalysts including iron, iron/aluminium, cobalt and cobalt/aluminium were tested. Experiments were also conducted examining how nanotube growth is affected by different thicknesses of catalyst. A good carbon precursor is ethanol vapour because ethanol is relatively safe and has been shown to produce high yields of SWNTs [21, 77]. All of our experiments were conducted using ethanol.

Nanotubes were typically grown on a *n*-doped silicon substrate with a thermally grown silicon dioxide layer ranging from 0.8 to 1.0 μm. This layer of silicon dioxide provides enough electrical insulation to allow for rapid SEM imaging. A catalyst film of cobalt, iron, aluminium or some combination of the metals was deposited on to the silicon dioxide using electron beam evaporation. Nominal catalyst thicknesses were one nanometre of each deposited metal however the thickness on some samples was varied. Samples were cleaved into pieces roughly 1.0 cm x 0.8 cm and placed into the growth chamber. Nanotubes were grown using thermal cold walled CVD at atmospheric pressure. Further details of the specifics of the growth reactor are presented in reference [22].

Most of the samples were patterned using a shadow masking technique. This technique generated 1-mm-diameter catalyst dots with a centre-to-centre spacing of 3 mm.

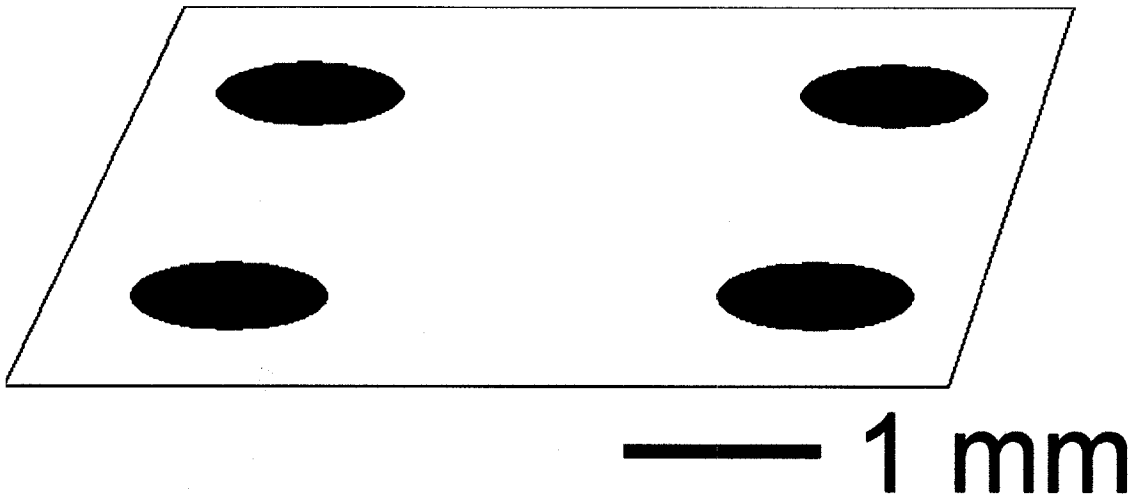

Figure 15 Typical catalyst pattern using shadow masking. The black dots indicate the location of the catalyst on top of the silicon substrate.

Growth recipes varied slightly depending on the specific experiment being performed. Specific recipes are explicitly explained in appendix B, however the following presents the general form of a typical growth. Samples containing an aluminium catalyst were initially preheated in air to 300°C for 10 minutes. This preheat in air oxidizes the aluminium layer of catalyst and has been shown to be an important step when using an iron/aluminium catalyst [22]. This step was found to have little effect on the grown nanotubes from samples with a catalyst of only cobalt. Next, the atmosphere of the reactor was replaced with a 2% hydrogen, balance argon gas. This was done by purging the reactor at a flow rate of 2.8 L/min for 5 minutes with straight argon and then another 5 minutes with 2% hydrogen, balance argon at the same flow rate. The hydrogen/argon flow rate was reduced to 0.6 L/min and the sample was heated. Various experiments were performed examining how adjustments to the sample temperature and ethanol concentration at different stages of the growth affected the product. Growth temperatures usually ranged from 600-900°C. Typical growths used a 10 minute hydrogen soak at the growth temperature before ethanol was introduced. This soak in

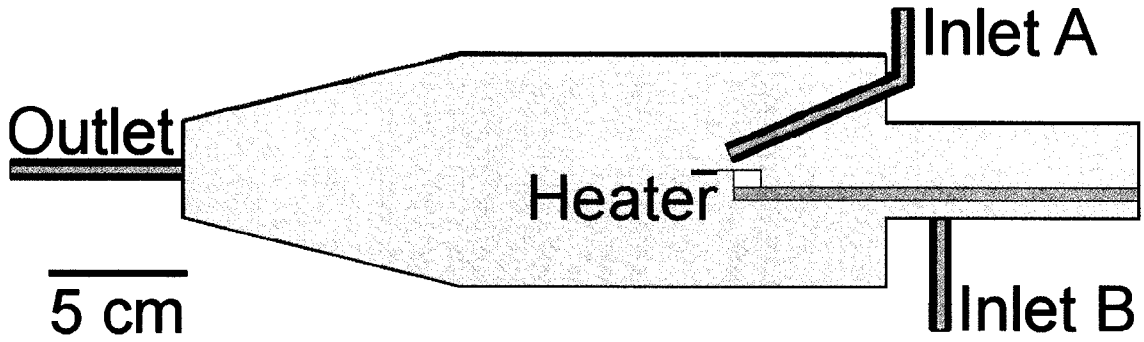

Figure 16 Scale cross sectional drawing of the reactor cavity. Gas can enter the reactor through either inlet A or inlet B. All gas leaves the reactor through the outlet.

hydrogen is thought to reduce any iron oxide to iron and allows for the formation of nanoparticles [22]. Ethanol was introduced for durations of 15 seconds to 30 minutes. This was done by diverting the hydrogen/argon gas at a typical flow rate of 0.6 L/min through an ethanol bubbler before it entered the reactor. After growth, the reactor was purged for 5 minutes at the growth temperature with a hydrogen/argon flow of 2.8 L/min before the sample was allowed to cool.

The reactor had two different inlets from which gas could enter. Generally, ethanol was introduced right next to the sample (inlet A) while high flow rate purges entered the inlet away from the sample (inlet B).

3.1 Measuring sample temperature

Two means of measuring the sample temperature were utilized. These include an optical pyrometer and a R-type thermocouple. The pyrometer measured the black body radiation given off by the sample and compared the relative intensities of two wavelengths. The thermocouple was inserted in a small hole at the base of the heater. The two independent means of measuring temperature where in rough agreement, but an offset which existed between them sometimes drifted during a growth run. The thermocouple measured the

temperature at the centre of the heater. The actual sample temperature varies with the thermal conductivity between the heater and the sample. The black body radiation measured by the pyrometer can be affected by the presence of catalyst and changes in the surface if large quantities of nanotubes are grown. Unless otherwise indicated, the pyrometer reading was used as the "true" temperature.

4 Growth temperature

4.1 Plan view

The growth temperature has been shown to have a large effect on nanotube properties including type, length, and yield (section 1.2). A series of different samples of CNTs were grown with modifications to the growth temperature. The catalyst for these experiments consisted of a 1 nm layer of iron on top of a 1 nm layer of aluminium. The specific growth recipe used to produce these samples is presented in the appendix section B.1. Optical images of the catalyst regions are shown in figure 17.

A blackening of the catalyst was observed after the lower temperature growths. Catalyst areas on samples grown at 550°C through 700°C appeared dark black optically with no magnification after growth. The degree of blackness decreased on grown samples as the growth temperature increased from 700°C. Samples grown at 800°C and above appeared identical optically with no magnification to samples not grown at all.

Some of growth temperature related effects can easily be observed by examining plan view SEM images of nanotubes grown at different temperatures (figure 18). Growing at 500°C (figure 18a) produced short (tens of nanometres) deposits. This sets a lower bound on the temperatures which our CVD technique can be used to grow nanotubes.

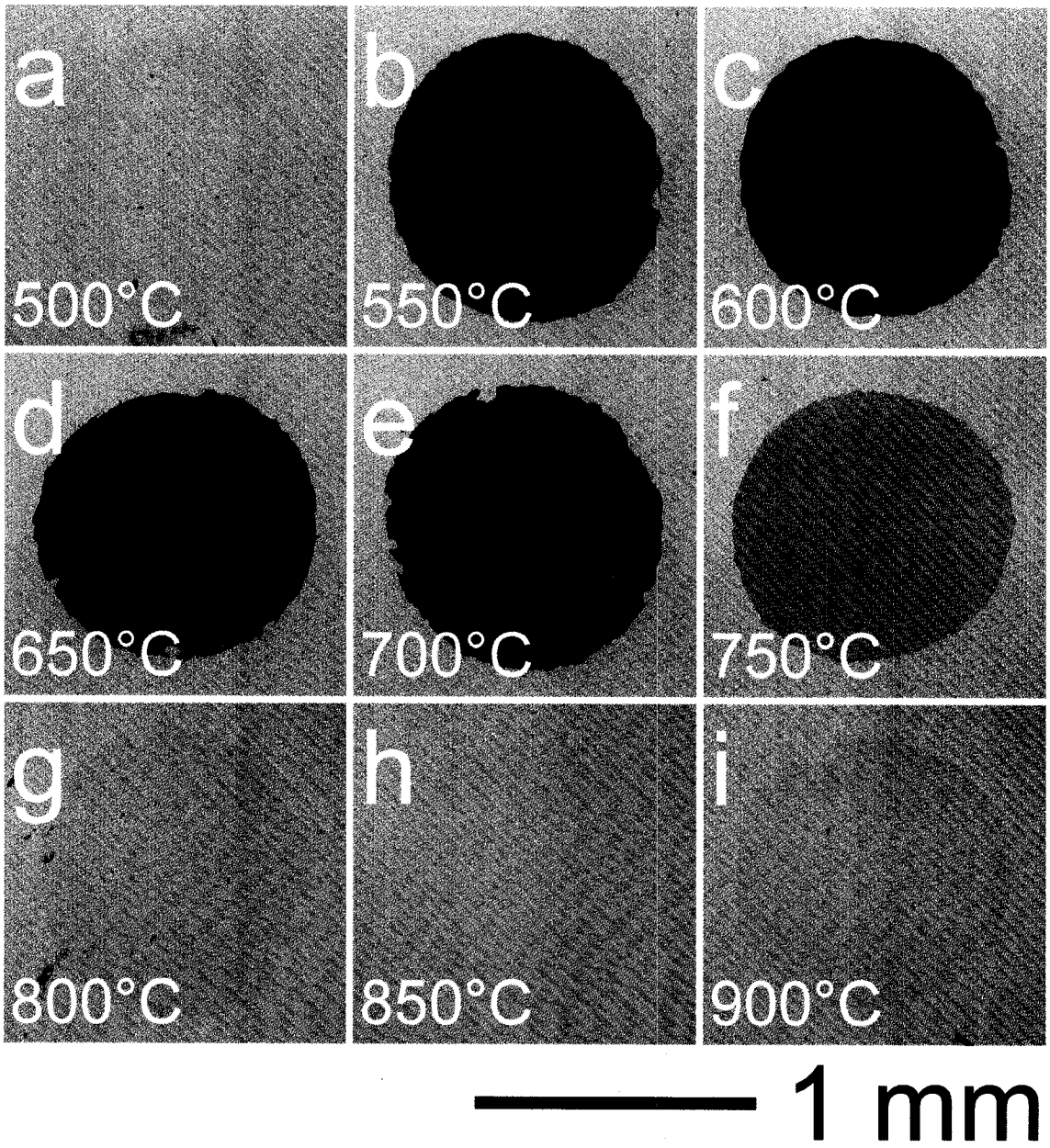

Figure 17 Optical images of the catalyst regions after growth. These images were taken with an optical microscope and a digital camera and were grown at the indicated temperatures. The growth temperatures were (a) 500°C, (b) 550°C, (c) 600°C, (d) 650°C, (e) 700°C, (f) 750°C, (g) 800°C, (h) 850°C, and (i) 900°C.

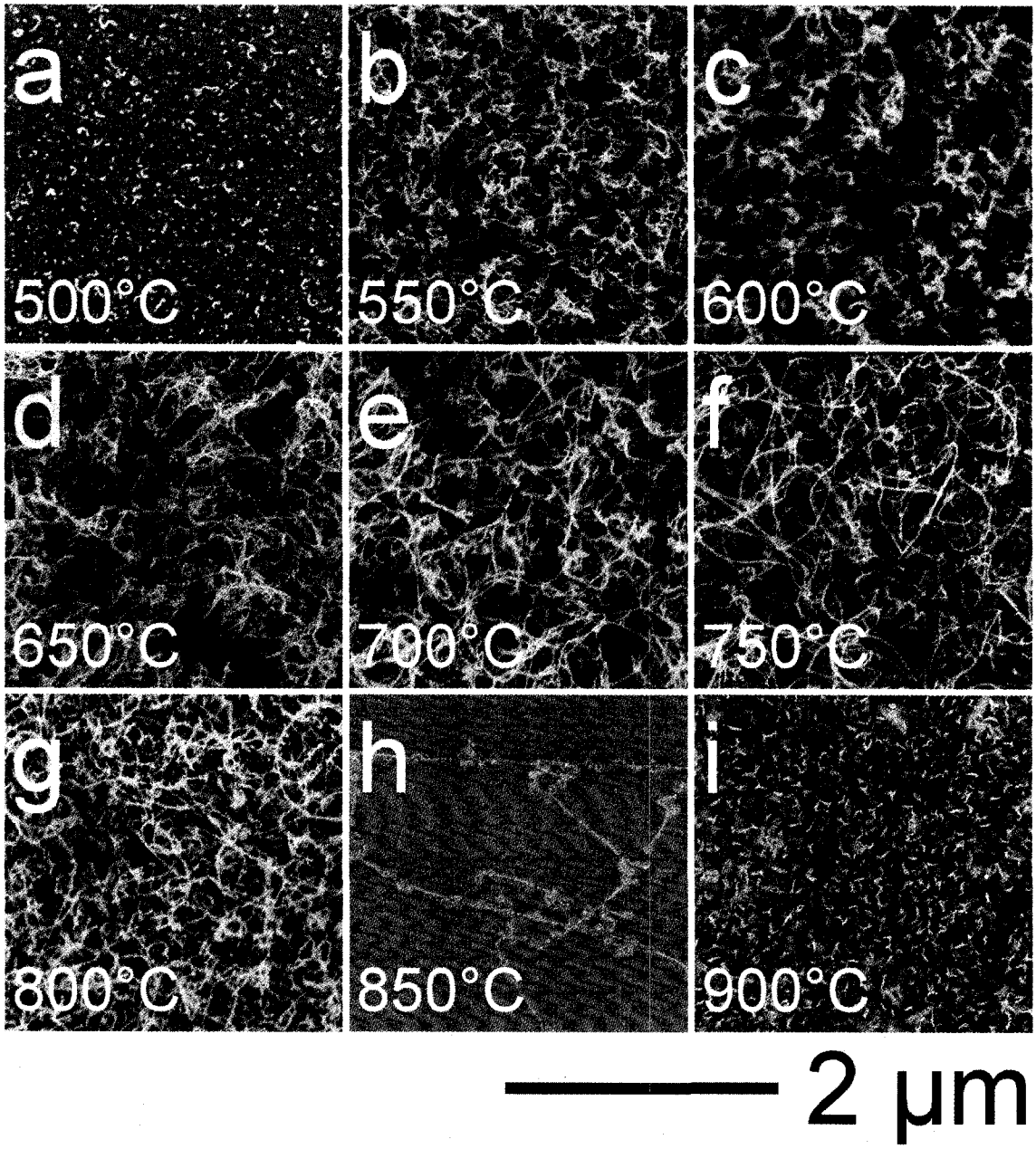

Figure 18 Plan view scanning electron microscope images taken at 1 kV for various growth temperatures [27]. The growth temperatures were (a) 500°C, (b) 550°C, (c) 600°C, (d) 650°C, (e) 700°C, (f) 750°C, (g) 800°C, (h) 850°C, and (i) 900°C.

Growth at 550°C resulted in the formation of a large amount of thick MWNTs (figure 18b). This can be observed through direct geometric contrast. These nanotubes as viewed in plan view appear short, on the order of a few hundred nanometres long. The growth directions of these nanotubes appear random and the nanotubes are very twisted. Here the degree of twist or straightness refers to the number of large variations in nanotube direction per unit length of the nanotube. Here we use this only as a qualitative description. It would be of interest to develop a more quantitative metric for comparing results. Also no underling catalyst or silicon dioxide can be seen through the nanotubes.

The visible length of the nanotubes grown at 600°C (figure 18c) is on the order of 500 nm. The degree of twist of the nanotubes is slightly less at this temperature. Here the substrate is not visible through the nanotubes. The diameter of the nanotubes is comparable with growth at lower temperatures.

The length of the visible nanotube segments from growth at 650°C (figure 18d) is approaching a micrometer. These nanotubes are straighter than their counterparts grown at lower temperatures. The layer of nanotubes is thick enough to completely hide the substrate. The diameter of the individual nanotubes is not noticeably different from the nanotubes grown at lower temperatures.

Increasing the growth temperature to 700°C (figure 18e) noticeably changes the grown nanotubes. Some of the visible segments of nanotube grown at this temperature are over a micron long. The nanotubes grown at 700°C are straighter than the ones grown at lower temperatures. The layer of nanotubes is thick enough to completely cover the substrate. The diameter of the nanotubes is roughly the same as the lower temperature growths.

Some of the visible segments of nanotubes grown at 750°C (figure 18f) are approaching two microns in length. The degree of twist is comparable to the 700°C. The nanotubes completely obscure the substrate. The nanotube diameter is not noticeably different than nanotubes grown at lower temperatures.

There is a large variation in the length of the nanotubes grown at 800°C (figure 18g). Some of the segments of nanotubes imaged in plan view at this temperature are multiple microns in length and some are only hundreds of nanometres. The substrate is visible through the layer of nanotubes. The density of the nanotubes is much less at 800°C than at the other lower temperatures which produced nanotubes. The diameter of the individual nanotubes grown at this temperature is again comparable to the growth at lower temperatures.

Growth at 850°C (figure 18h) produced SWNT candidates. A SWNT candidate refers to a nanotube which appears in SEM to be thin like a SWNT but has not been proven to be single walled using a rigorous technique, for example Raman spectroscopy. It is more difficult to observe these thin nanotubes through geometric contrast due to their size. When viewed in SEM at low accelerating voltages (1 kV), charging effects of the silicon dioxide highlight the area around the thin surface nanotubes (see section 2.1). This allows for simplified viewing of these thin nanotubes, however it makes direct measurement of diameters difficult. The density of the nanotubes on the substrate is very low resulting in the substrate comprising the vast majority of the imaged area. The nanotubes grown at 850°C are long (~ 10 microns) and straight.

Samples grown at 900°C (figure 18i) or above appeared similar to samples grown at 500°C. These samples contained short deposits not useful for manufacturing devices.

There was some variation in this upper cut-off temperature depending on the particular catalyst used and other growth parameters. Some samples were grown at 900°C which contained thin SWNT candidates.

4.2 Side view

In addition to altering the properties of individual nanotubes, growth temperature was found to affect the nanotube collective arrangement. This can easily be noticed by examining side view SEM images (figure 19). The edge of the catalyst is examined at an inclined angle (similar to figure 7) for samples grown at different temperatures. The alignment and the forest height are both significantly affected by the growth temperature.

The sample grown at 500°C contained a very low concentration of nanotubes. Its side view image is not shown. Growth at 550°C (figure 19a) was shown to produce many thick MWNT. These nanotubes are very twisted but show some indications of alignment in the vertical direction. The height of the nanotube forest is on the order of one micrometer. Samples growth at 600°C (figure 19b) produced tall vertically aligned forests. The height of the forest was measured to be around 7 μm. Nanotubes growth at 650°C (figure 19c) also produced a tall vertically aligned forest. The height of this forest was slightly less measuring in at 6.5 μm. Growth at 700°C (figure 19d) produced forests of nanotubes with poor alignment. The height of the forest was on the order of a micrometer. Nanotubes growth at 750°C (figure 19e) also show little alignment. The height of this nanotube arrangement was roughly half of a micrometer. Samples grown at temperatures above 750°C tended to lie on the substrate and were found in lower concentrations. As a result, side view images are not shown.

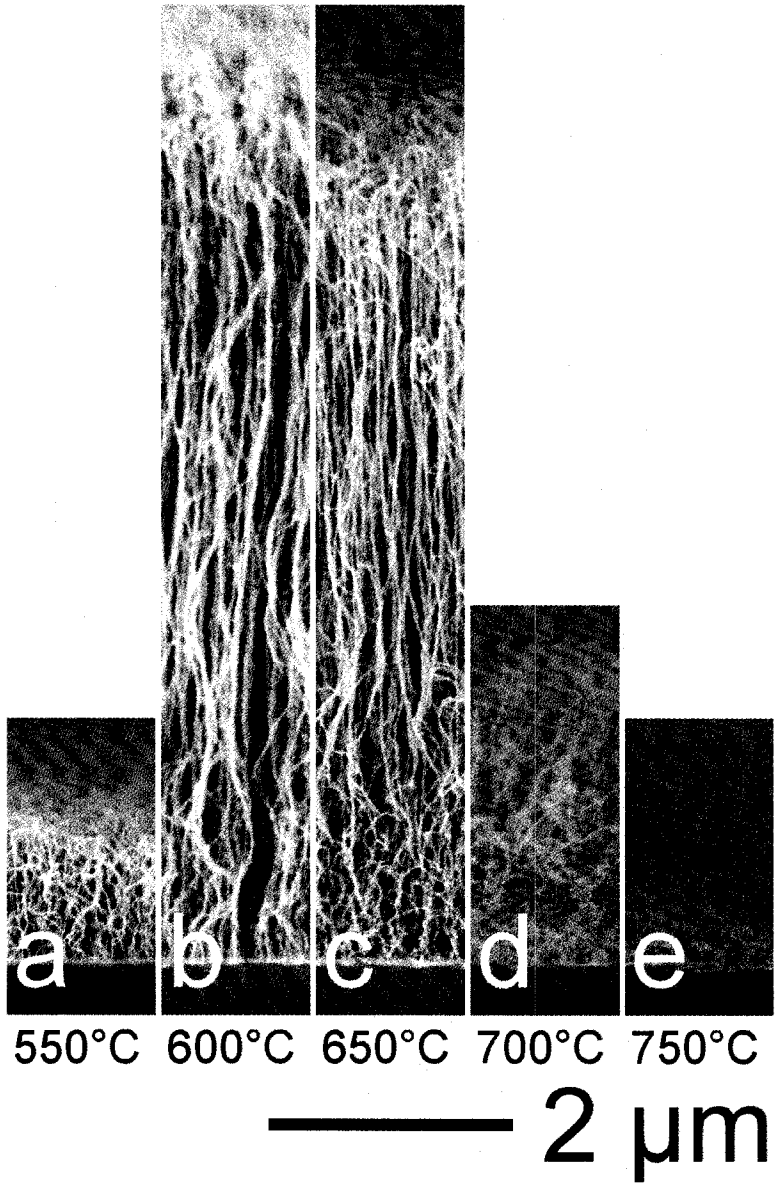

Figure 19 Side view scanning electron microscope images for various growth temperatures [27]. Each sample was tilted approximately 85° from the normal and imaged at 1 kV. The growth temperatures were (a) 550°C, (b) 600°C, (c) 650°C, (d) 700°C, and (e) 750°C.

4.3 Raman spectroscopy

The Raman spectra (see section 2.3) of samples grown from 500-900°C were measured and examined. The excitation wavelength was 632.8 nm. The concentration of radial breathing modes (RBMs) was found to be dependent on the growth temperature. A RBM is strong evidence that a resonant SWNT is present. For each sample, the Raman

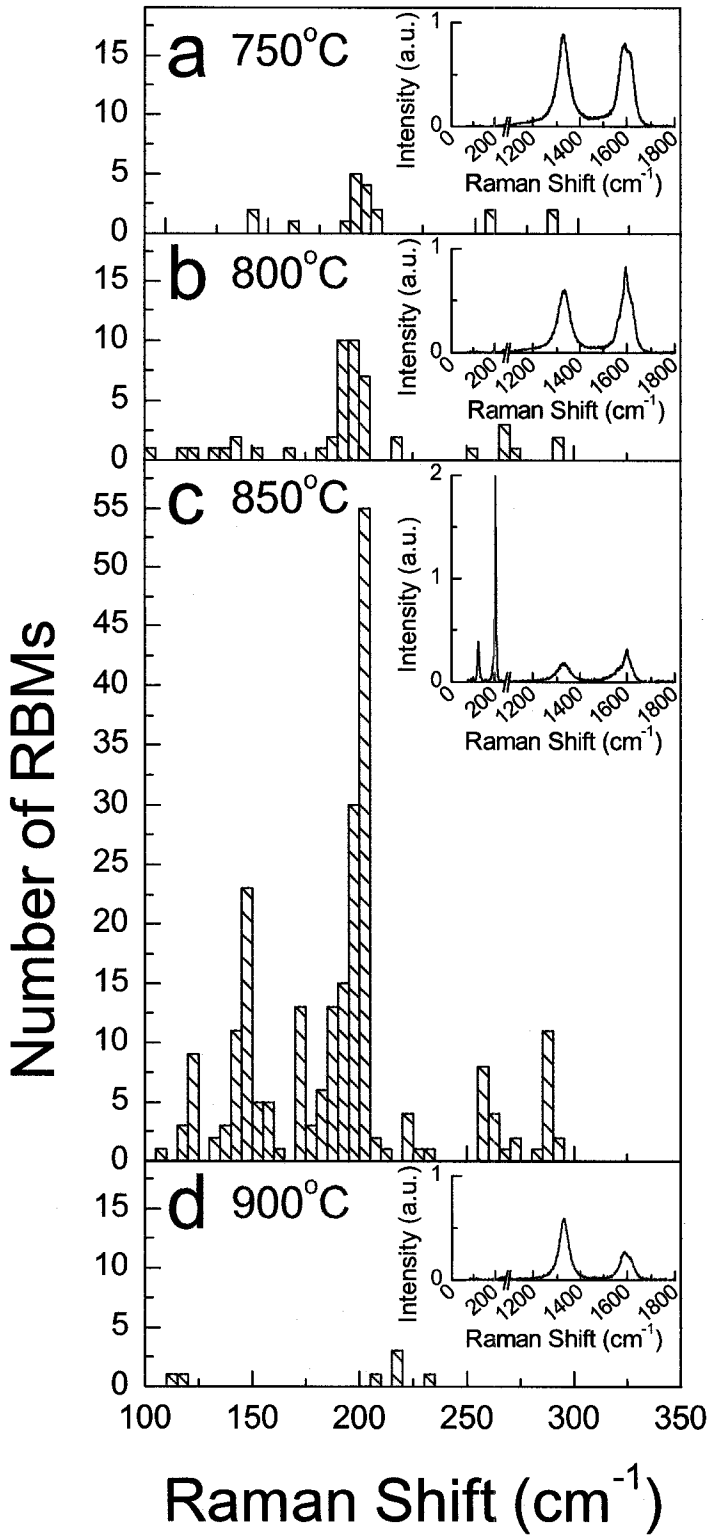

Figure 20 Histogram of abundance of radial breathing modes (RBMs), given a sampling size of one hundred spots as a function of growth temperature [27]. The insets show the RBM, D and G band energy ranges of a typical Raman spectra for the various temperatures. All spectra were obtained with 632.8 nm excitation. The growth temperature of the sample was (a) 750°C, (b) 800°C, (c) 850°C, and (d) 900°C. There were on average (a) 0.19, (b) 0.48, (c) 2.4, and (d) 0.07 RBMs per ~1 μm diameter laser spot.

spectra from one hundred spots spaced at least 15 μm apart and roughly 1 μm in diameter was taken. Figure 20 shows the histograms of the frequency shift of the RBMs. A RBM was taken to be any sharp peak in the range 100 cm^{-1} to 300 cm^{-1} [68]. These peaks were binned in 5 cm^{-1} increments. There was a large variation in the number of RBMs found at the different growth temperatures. Typical nanotube Raman spectra including the D, G and RBM bands for the various temperatures are shown as insets.

The largest number of RBMs found occurred at a frequency of around 200 cm^{-1}. This frequency corresponds to a nanotube diameter of roughly 1.2 nm (refer to section 2.3). This number is roughly independent of the temperature the nanotubes were grown at. There were RBMs throughout the 100-300 cm^{-1} range indicating a large variety in SWNT diameter.

No RBMs were found from growth at temperatures below 750°C. Growth at 750°C (figure 20a) was found to produce on average 0.19 RBMs per laser spot. Samples grown at 800°C (figure 20b) had on average 0.48 RBMs per laser spot. Growth at 850°C (figure 20c) produced on average 2.4 RBMs per laser spot. Nanotubes grown at 900°C (figure 20d) were found to have on average 0.07 RBMs per laser spot.

The highest concentration of RBMs found using this growth technique was at a growth temperature of 850°C. This is clearly shown by figure 21 which is a plot of the temperature dependence of RBMs.

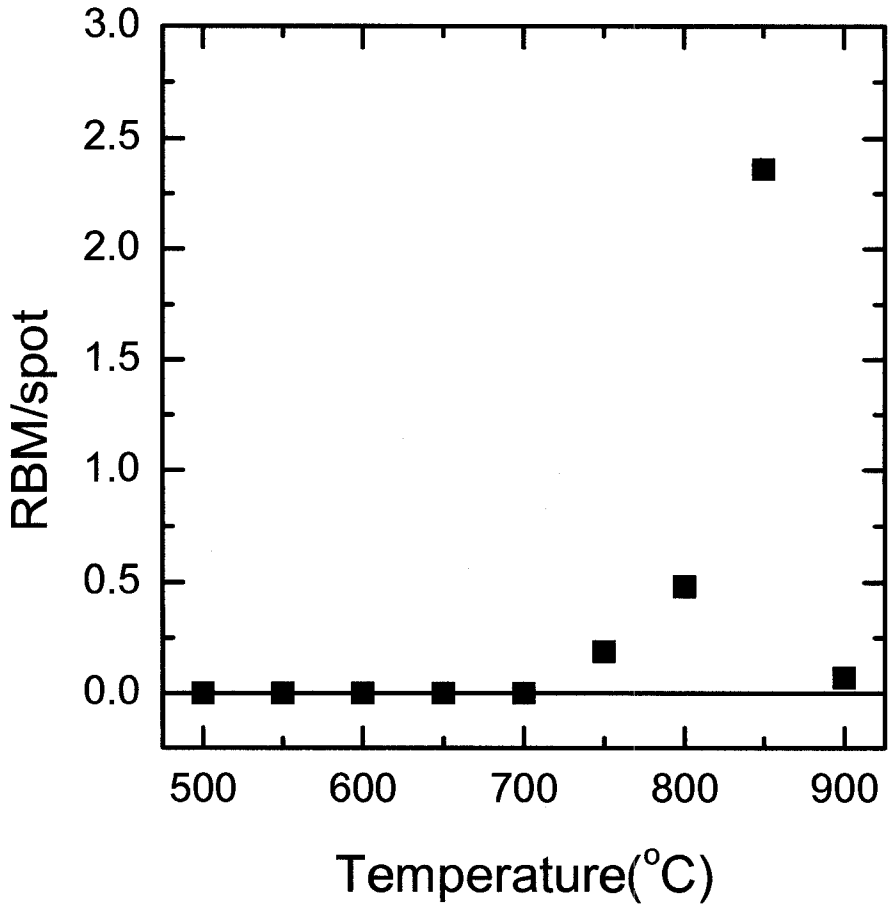

Figure 21 Radial breathing mode concentration dependency on growth temperature. The highest concentration of radial breathing modes occurs at a growth temperature of 850°C.

The ratio of the D band over the G band is shown in figure 22. The circles represent the ratio of the absolute intensity of the peaks. The squares show the ratio of the peaks after the removal of a linear baseline to account for variations in the background noise at different frequencies. The lowest D to G band ratio from both plotting techniques occurs at 850°C. This suggests that of all of the growth temperatures examined, growth at 850°C produced nanotubes with the least amount of disorder.

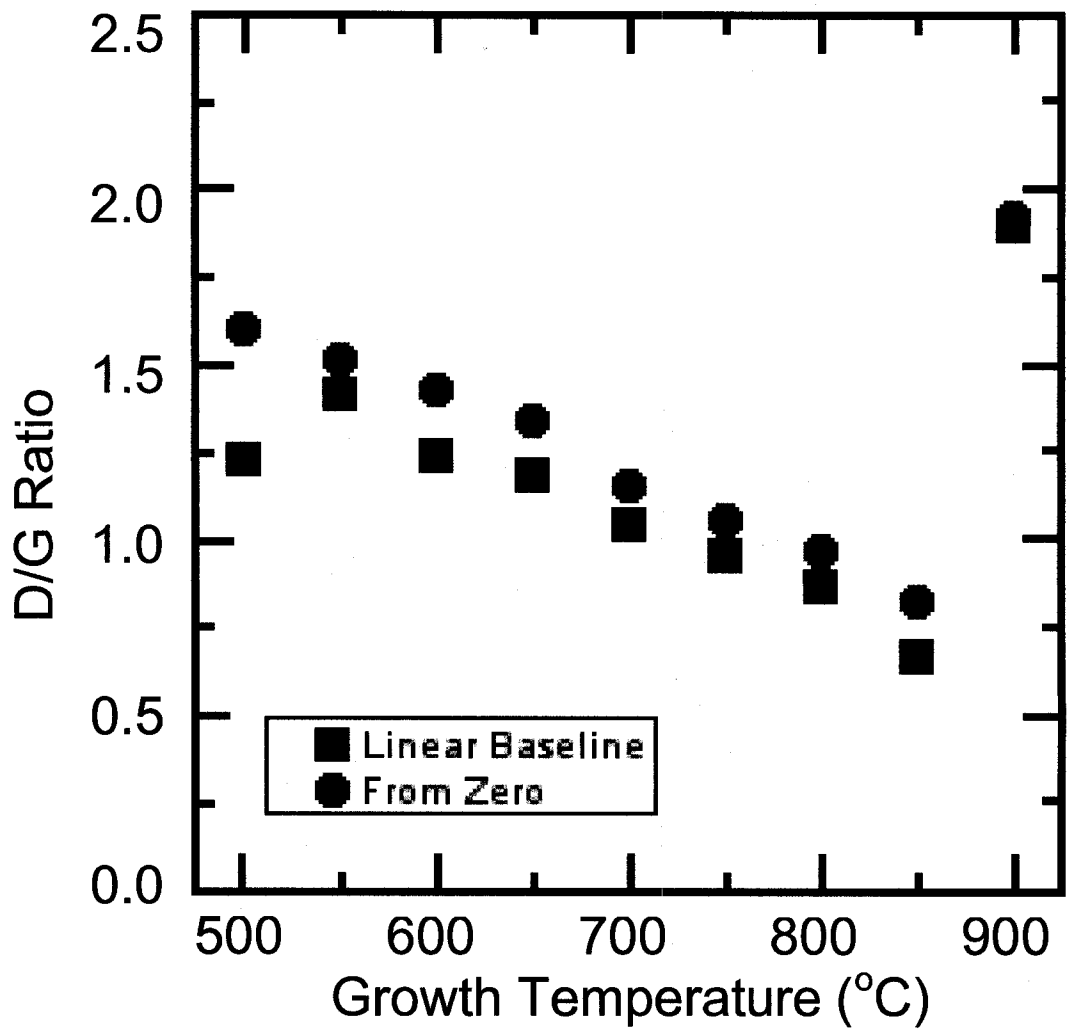

Figure 22 Variations in nanotube D and G bands with respect to growth temperature. The lowest ratio occurs at a growth temperature of 850°C.

4.4 Discussion

There are only subtle variations which can be observed in plan view SEM between the samples grown from 550-750°C (figure 18). Plan view SEM only reveals information with respect to the top of the nanotube forest. Examining the same samples with side view SEM reveals that there are large variations in the collective arrangement of the nanotubes grown at these temperatures. The highest most vertically aligned forests are grown in the range of 600-650°C. The Raman examination of this temperature range did

not contain any RBMs. This absence of RBMs combined with the large diameters viewed in SEM allows us to conclude that these tall forests consist primarily of MWNTs.

RBMs are found to be more abundant as the growth temperature increase from 750°C. The concentration of RBMs peaks at growth temperatures of 850°C. At 850°C the concentration of RBMs is so high that on average more than one RBM was found per spot. The D to G band ratio was also lowest at 850°C which is evidence that the concentration of defects was at its lowest level at this growth temperature. There were few thick MWNTs visible in the plan view SEM images of the samples grown at this temperature. These results suggest that the highest concentration of SWNTs of all of the temperatures examined occurs at 850°C.

5 Hydrogen soak

One component of the goal of this project is to produce high yields of SWNT. It was discovered that large quantities of MWNT could be produced by growing at low temperatures (650°C). Also low quantities of SWNT could be produced by growing at high temperatures (850°C). Our effort to explain these results with respect to nanoparticle formation lead to the development of a new set of experiments.

The thin film metal catalyst breaks up into nanoparticles at the high nanotube growth temperatures (section 1.3). We hypothesized that large nanoparticles exist at low temperatures (600°C) and account for the growth of thick MWNT. In contrast, we hypothesized that small nanoparticles exist at high temperatures (850°C) and produce thin SWNT candidates. If a sample was heated to a high temperature (850-900°C) small nanoparticles should form. It was thought that if the sample was quickly cooled to a lower temperature (600°C) then the growth mechanism which accounts for the high yields could result in the production of large amounts of SWNTs. Experiments were conducted to test this hypothesis. The growth recipe is presented in the appendix section B.2. The results of these experiments are shown in figures 23 through 25. For clarity purposes samples are referred to using a *hydrogen soak temperature/grow temperature* notation. For example, a sample soaked in hydrogen at 850°C and then quickly cooled to 600°C before ethanol was introduced is noted by 850°C/600°C.

5.1 Hydrogen soak at 850°C

The 850°C/600°C sample (figure 24a) produced very few nanotubes. The few nanotubes observed from this growth technique were all thick MWNT.

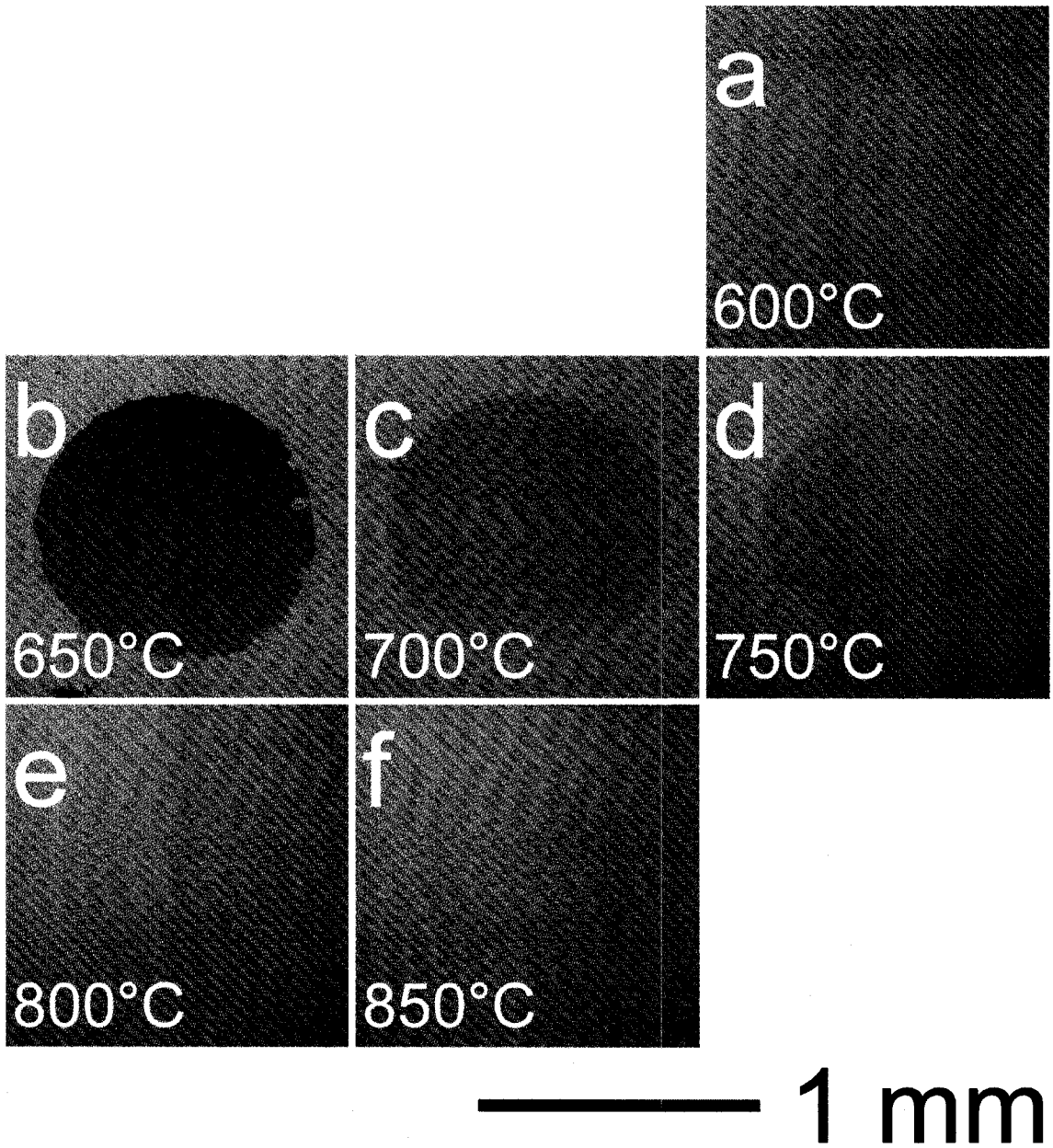

Figure 23 Optical images of the catalyst after 850°C hydrogen soak and growth. The growth temperatures of the samples were (a) 600°C, (b) 650°C, (c) 700°C, (d) 750°C, (e) 800°C and (f) 850°C.

Nanotubes from the 850°C/650°C (figure 24b) growth appear similar in SEM to nanotubes both soaked in hydrogen and grown at 650°C (figure 18d). The 850°C/650°C sample is however optically not as black as the sample both soaked in hydrogen and grown at 650°C. This suggests that the layer of nanotubes is thinner on the high temperature soaked sample. Both samples contain thick MWNT.

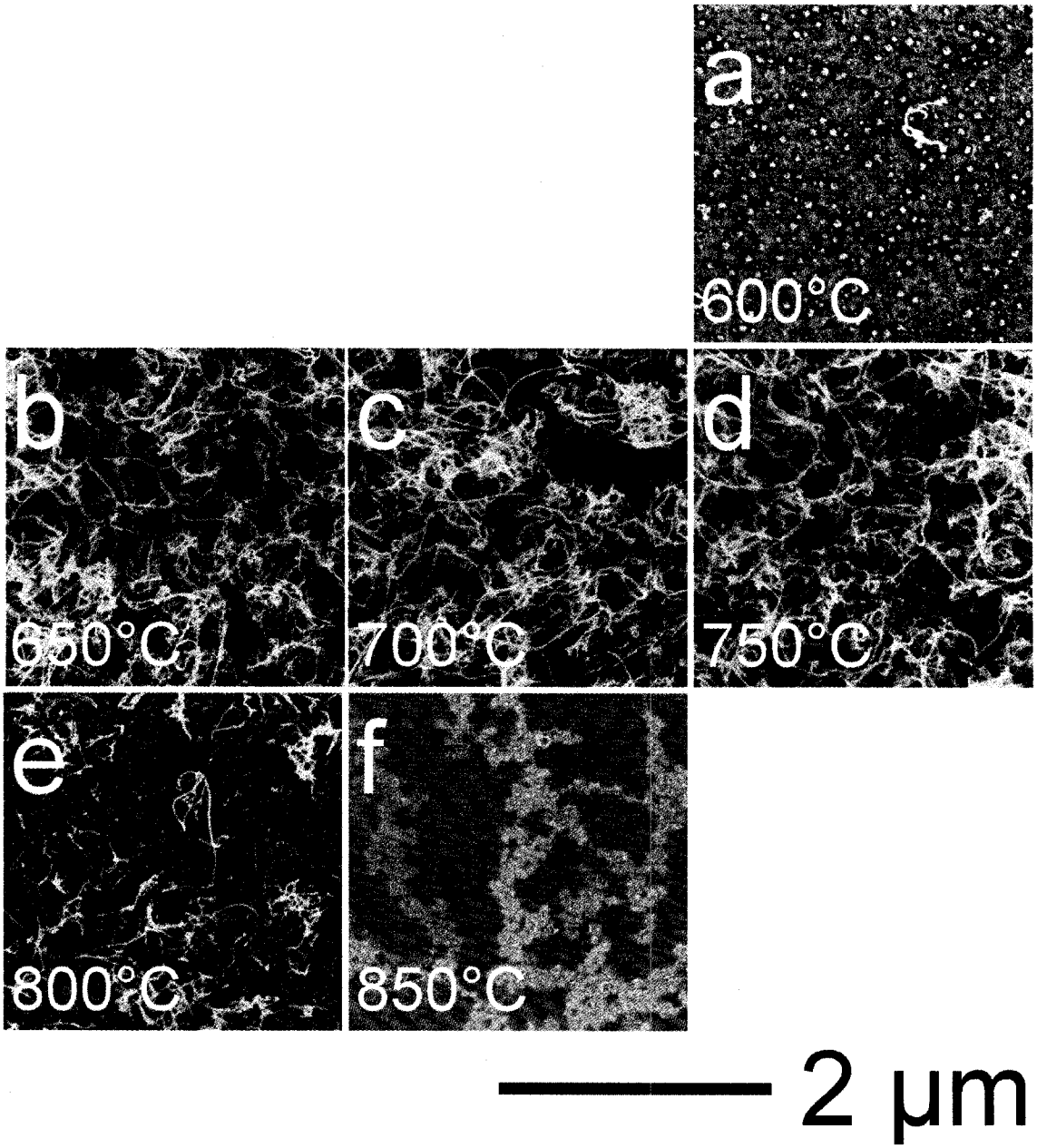

Figure 24 Hydrogen soak at 850°C. Samples were heated to 850°C for the 10 minute soak in hydrogen and then quickly (within 30 seconds) cooled to the growth temperature (indicated on the images) and ethanol was introduced into the reactor for 20 minutes. The growth temperatures were (a) 600°C, (b) 650°C, (c) 700°C, (d) 750°C, (e) 800°C and (f) 850°C. Scanning electron microscopy images were taken at 1 kV.

The 850°C/700°C sample (figure 24c) also appears very similar in plan view SEM to the corresponding sample grown without the high temperature hydrogen soak. The

optical appearance of the high temperature hydrogen soak sample was lighter in colour than the sample soaked in hydrogen at 700°C.

The catalyst can be seen though the nanotubes of the 850°C/750°C sample (figure 24d) while it can not be seen on the sample soaked in hydrogen and grown at 750°C.

Growing at 850°C/800°C (figure 24e) resulted in the formation of fewer nanotubes than were found on the sample both soaked in hydrogen and grown at 800°C.

The 850°C/850°C sample (figure 24f) was grown identical to the previous growth at 850°C (figure 18h). Both samples contain thin likely SWNT. There is a difference in the charge diffusion length of the substrate around the nanotube (section 2.1). A larger amount of substrate is charged (on figure 24f) highlighting the nanotubes further however making their diameters more difficult to determine.

5.2 Hydrogen soak at 900°C

The 900°C/600°C, 900°C/650°C and 900°C/700°C growths (figure 25a, b, c) produced very few nanotubes. The few nanotubes on the samples are all short (<1μm) and thick MWNT. The catalyst on all of the growths soaked in hydrogen at 900°C appears identical optically before and after growth. Therefore optical images are not shown.

The 900°C/750°C growth (figure 25d) produced very few nanotubes in general. The nanotubes present on this sample are SWNT candidates.

Nanotubes grown on 900°C/800°C samples (figure 25e) are SWNT candidates. There are few nanotubes on this sample however there are more than were found on the samples soaked in hydrogen at 900°C and grown at lower temperatures.

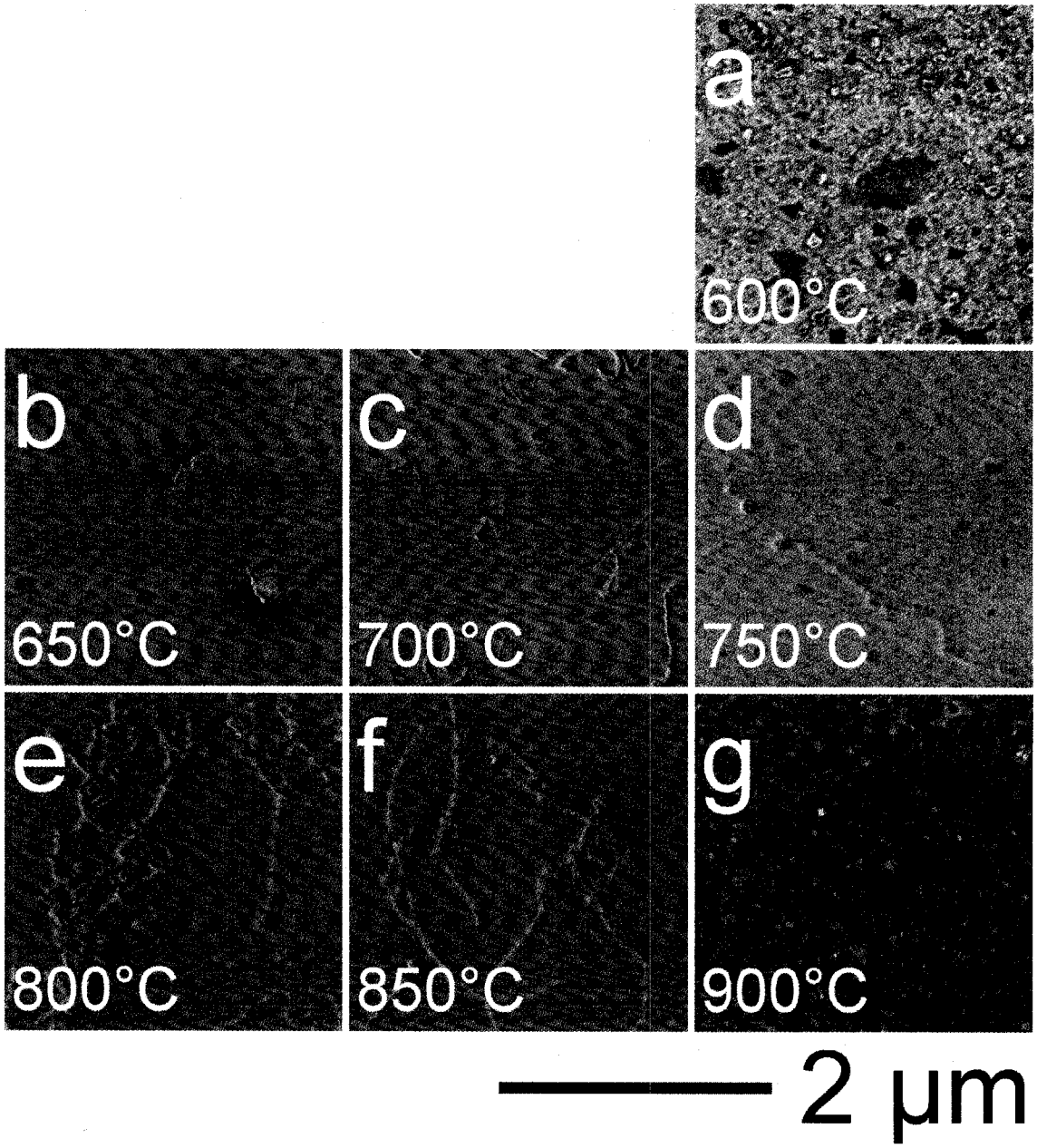

Figure 25 Hydrogen soak at 900°C. Samples were heated to 900°C for the 10 minute soak in hydrogen and then quickly (within 30 seconds) cooled to the growth temperature and ethanol was introduced into the reactor for 20 minutes. The growth temperatures were (a) 600°C, (b) 650°C, (c) 700°C, (d) 750°C, (e) 800°C, (f) 850°C and (g) 900°C. SEM images were taken at 1 kV.

The 900°C/850°C sample (figure 25f) contained SWNT candidates. This sample appears very similar to the previous growth at 850°C which also produce SWNT

candidates. The temperature range around 850°C appears to be the ideal range for growing SWNTs.

The 900°C/900°C growth (figure 25g) was identical to the previous growth at 900°C (figure 18h). Very few nanotubes were found on either sample. The Raman spectrum from the previous growth at 900°C contains some RBMs (figure 20d). It is expected that there is a low concentration of SWNTs on this 900°C/900°C sample.

5.3 Discussion

There is a large difference in the nanotubes on samples which were soaked in hydrogen at their growth temperature, at 850°C and at 900°C. Samples soaked and grown at the same low temperature (600-750°C) produced dense forests. Samples soaked in hydrogen at 850°C and then grown at a low temperature produced forests with lower density. Samples soaked in hydrogen at 900°C and then grown at a lower temperature did not produce forests. Soaking samples at high temperatures reduced the number of MWNTs grown. The concentration of SWNT did not increase by soaking at high temperatures and then growing at a slightly reduced temperature. The hydrogen soaking experiments were not pursued further because SWNT yields were reduced not increased as we predicted. Heating the samples is clearly not reversible.

6 Nanoparticles

In an attempt to gain a better understanding for why temperature has such a large effect on nanotube growth, the catalyst behaviour at different temperatures was examined. Samples were prepared similar to those previously detailed with one exception. No ethanol was introduced into the reactor. The heat was turned off at the point that ethanol was introduced in previous runs and the sample was cooled as quickly as possible to room temperature. The specific recipe uses an iron/aluminium catalyst and is detailed in the appendix section B.3. It was assumed that the catalyst was stable at room temperature. It was also assumed that if cooling occurred quickly, the size of the catalyst would remain similar to its high temperature state although its morphology may change. Figures 26 and 27 display the results of this nanoparticle study.

6.1 Plan view SEM

Samples heated to 600°C, 650°C, 700°C and 750°C (figures 26a, b, c, d) did not contain any nanoparticles visible in SEM. Some sort of surface contamination, most likely a particulates of dust were used to focus these images, which revealed that these substrates were very smooth. This indicates that our thin catalyst film did not break up into nanoparticles at these temperatures.

Heating to above 800°C (figure 26e, f, g) resulted in the formation of nanoparticles. A variety of sizes of nanoparticles were produced at these temperatures. The sizes of the nanoparticles varied depending on the specific temperature the sample was heated to.

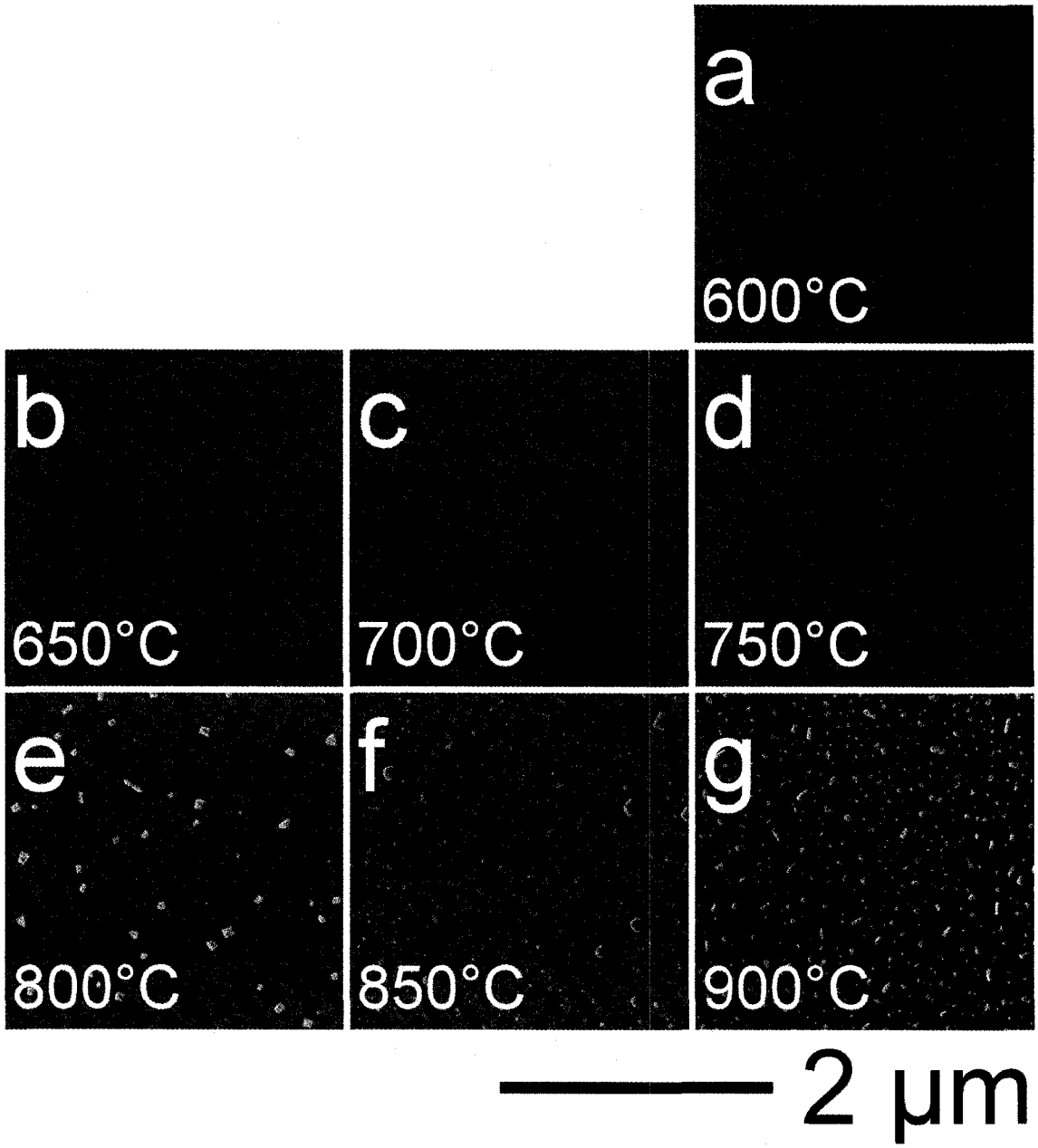

Figure 26 Plan view scanning electron microscope images of nanoparticles. Iron/aluminium samples were heated to various growth temperatures however no ethanol was introduced into the reactor. The temperatures were (a) 600°C, (b) 650°C, (c) 700°C, (d) 750°C, (e) 800°C, (f) 850°C and (g) 900°C. Images were taken with an accelerating voltage of 5 kV.

6.2 Histogram of nanoparticles

Histograms of nanoparticle size were generated using UTHSCSA ImageTool software. Nanoparticles within the SEM images were identified based on differences in between the shading of the nanoparticles and the background. The number of pixels used to

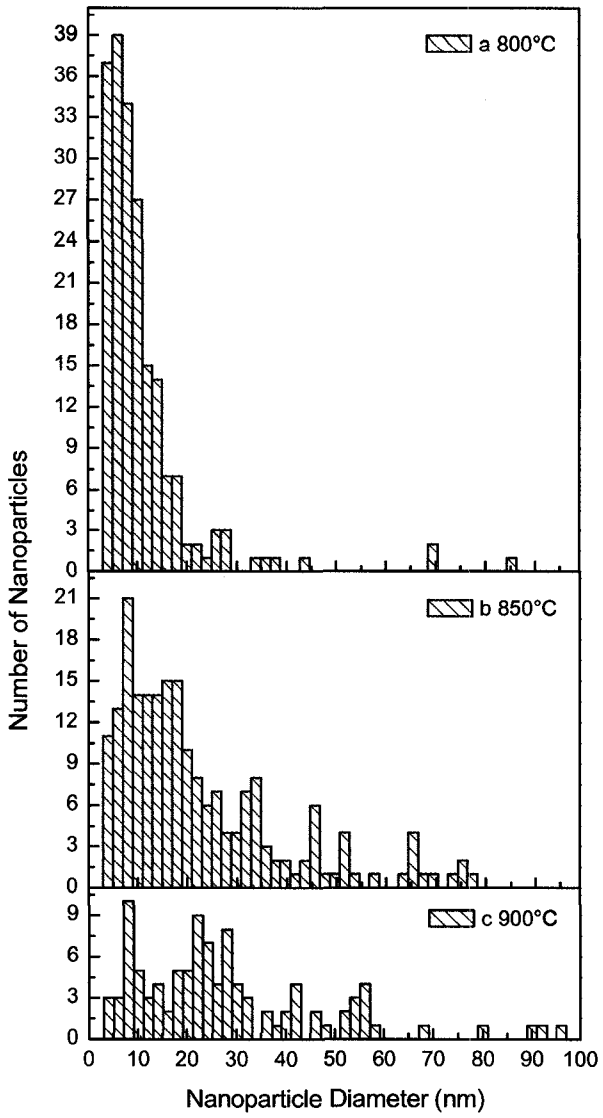

Figure 27 Histogram of the nanoparticle size distribution of the samples depicted in figure 26. The samples were heated to (a) 800°C, (b) 850°C and (c) 900°C. The sample area use d to generate the histograms is 0.74 μm^2.

represent each nanoparticle was then counted. This allows for an estimation of the various nanoparticle sizes. The images presented in figure 26 show the larger nanoparticles (30-50 nm diameter). Higher magnification SEM images than those shown in figure 26 were used to generate the following histograms.

The thin catalyst film remains smooth until the temperature reaches around 800°C. At this temperature, a large number of very small nanoparticles (3-15 nm in

diameter) form. At 850°C the nanoparticle distribution changes and larger nanoparticles (15-30 nm in diameter) are more common. At 900°C there are many even larger nanoparticles ranging in size from 30-50 nm. Above 800°C the average nanoparticle size increases with temperature. Other groups have also reported that average nanoparticle diameter of an iron/aluminium catalyst increases with sample temperature [43].

It is hypothesized that the small (<15 nm diameter) nanoparticles are responsible for producing single walled nanotubes. These small nanoparticles are very uncommon below temperatures of 750°C coinciding with no single walled nanotubes grown below this temperature (figure 20). Above this temperature, both the concentration of small nanoparticles and SWNTs increase until 850°C. At higher temperatures the average nanoparticle size is larger and the concentration of SWNTs decreases.

At lower temperatures (600°C – 750°C) the catalyst appears smooth in the SEM images. The catalyst remains a thin film at low growth temperatures. The growth of the MWNT forests is not initiated from nanoparticles but this film. This partially explains the results shown in figures 24 through 25. Soaking samples in hydrogen to 850°C causes the thin catalyst film to break up. The number of growth sites for the MWNT forest is reduced and so the forest growth less dense. Soaking samples at 900°C in hydrogen resulted in much of the catalyst film breaking up into nanoparticles. This accounts for the lack of MWNT growth noticed at lower temperatures in figure 25. Nanoparticle size however does not explain the concentration of SWNTs in these figures. Soaking in hydrogen at high temperatures to produce small nanoparticles and then growing at low temperatures produced few if any SWNT candidates (figure 25 a, b & c). More experimentation must be performed to explain these results.

7 Catalyst thickness

All of the previously explained results were from samples grown on an iron aluminium catalyst. Literature indicates that cobalt is also useful catalyst for producing high yields of SWNT [30]. Experiments were conducted using cobalt in an attempt to improve nanotube yields. A series of samples were grown at different temperatures on samples with a catalyst consisting of 1.0 nm of aluminium and different thicknesses of cobalt. The growth recipe is identical to the one in the appendix section B.1. The results from this experiment are shown in figures 28-31. The following section uses a *cobalt thickness/growth temperature* notation. For example, a sample grown on a catalyst with a cobalt thickness of 1.0 nm and a growth temperature of 600°C is referred to as 1.0 nm/600°C.

7.1 Plan view SEM

The 1.0 nm/600°C growth produced a thick nanotube forest. The substrate is not visible through the nanotubes. Growth on 0.1 nm/600°C resulted in a much more sparse nanotube forest. The substrate can easily be found through the forest. Growth on 0.02 nm/600°C produced very few nanotubes at all.

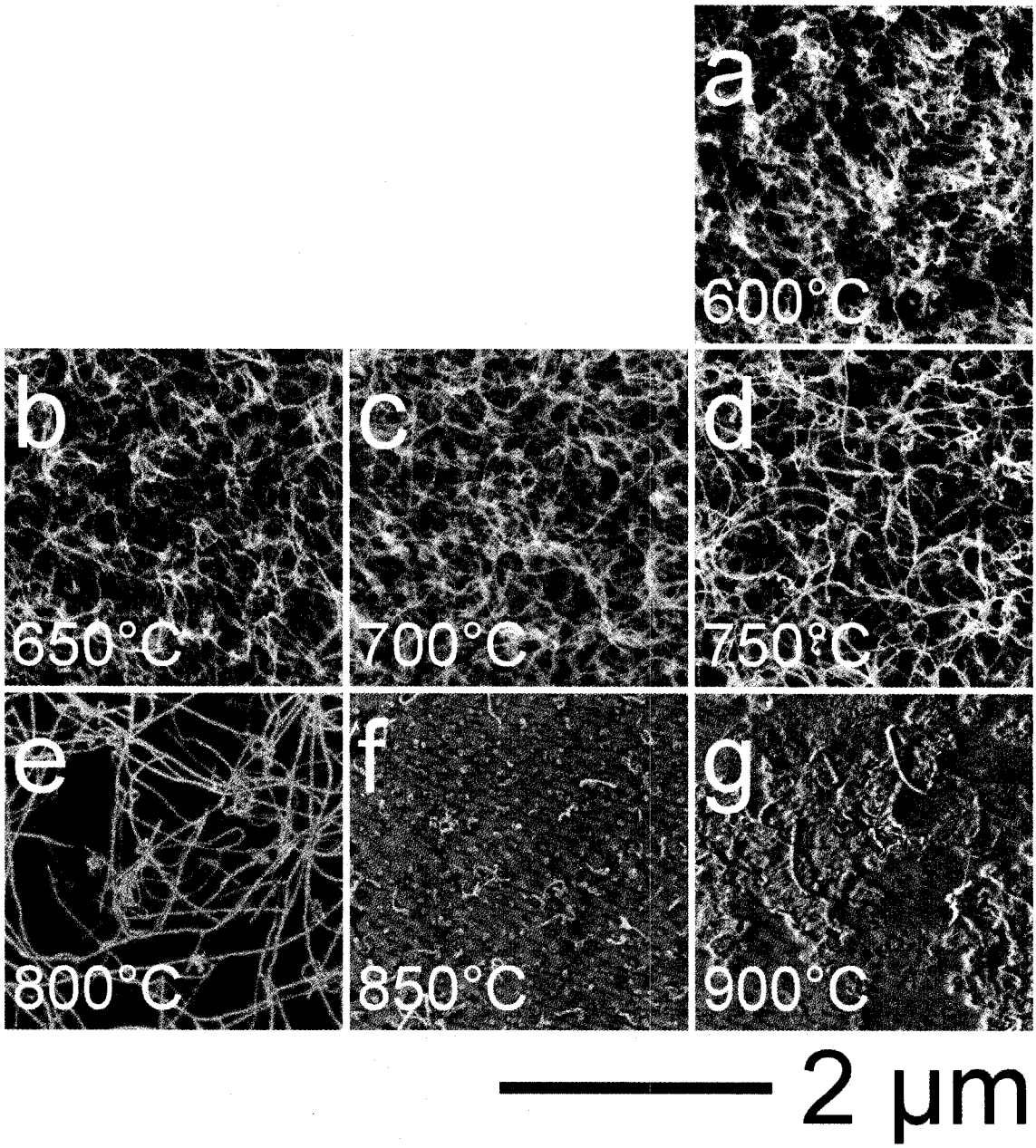

Figure 28 Growth on a 1.0 nm cobalt, 1.0 nm aluminium catalyst taken at 1 kV for various growth temperatures. The growth temperatures were (a) 600°C, (b) 650°C, (c) 700°C, (d) 750°C, (e) 800°C, (f) 850°C and (g) 900°C.

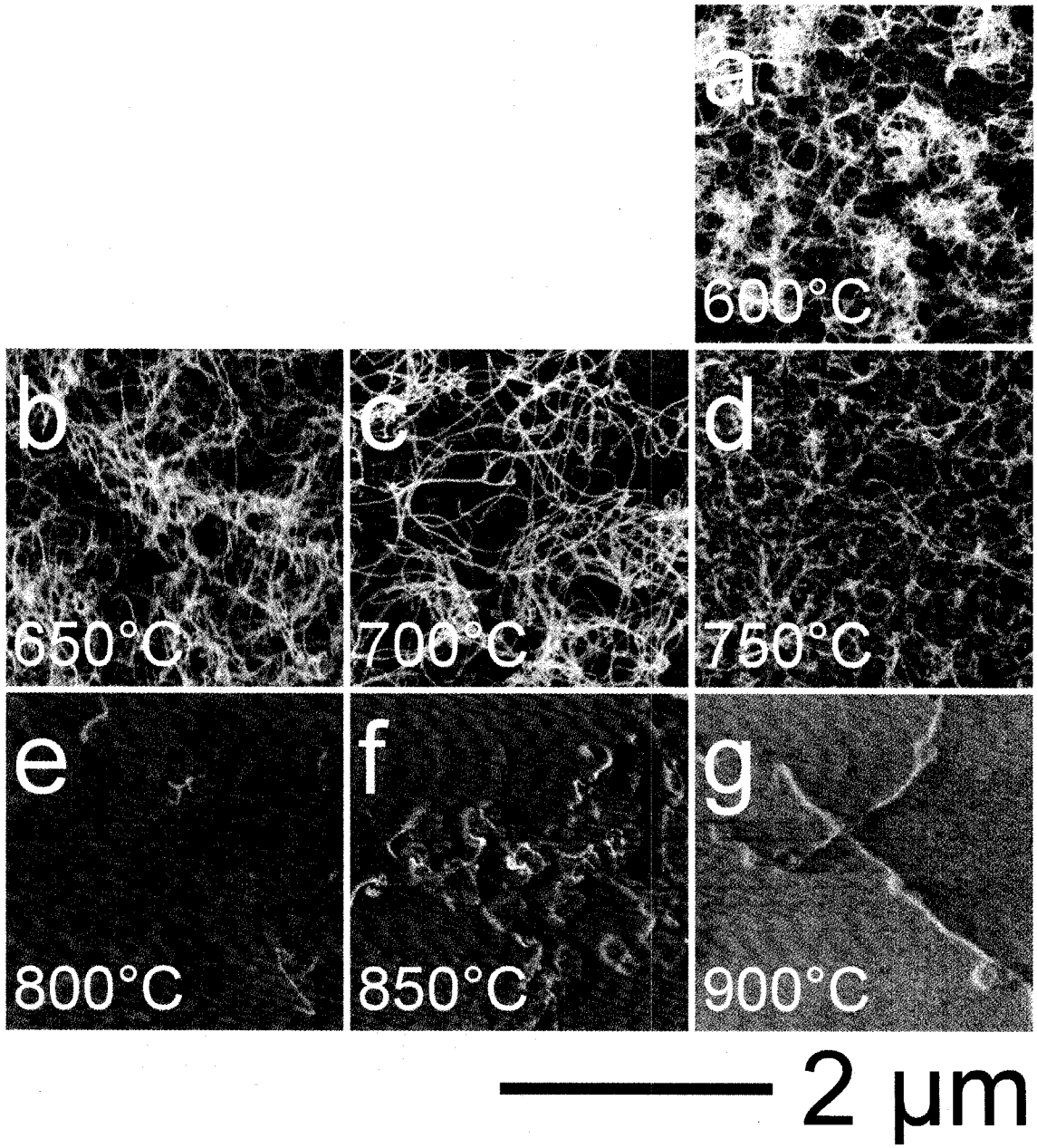

Figure 29 Growth on a 0.1 nm cobalt, 1.0 nm aluminium catalyst taken at 1 kV for various growth temperatures. The growth temperatures were (a) 600°C, (b) 650°C, (c) 700°C, (d) 750°C, (e) 800°C, (f) 850°C and (g) 900°C.

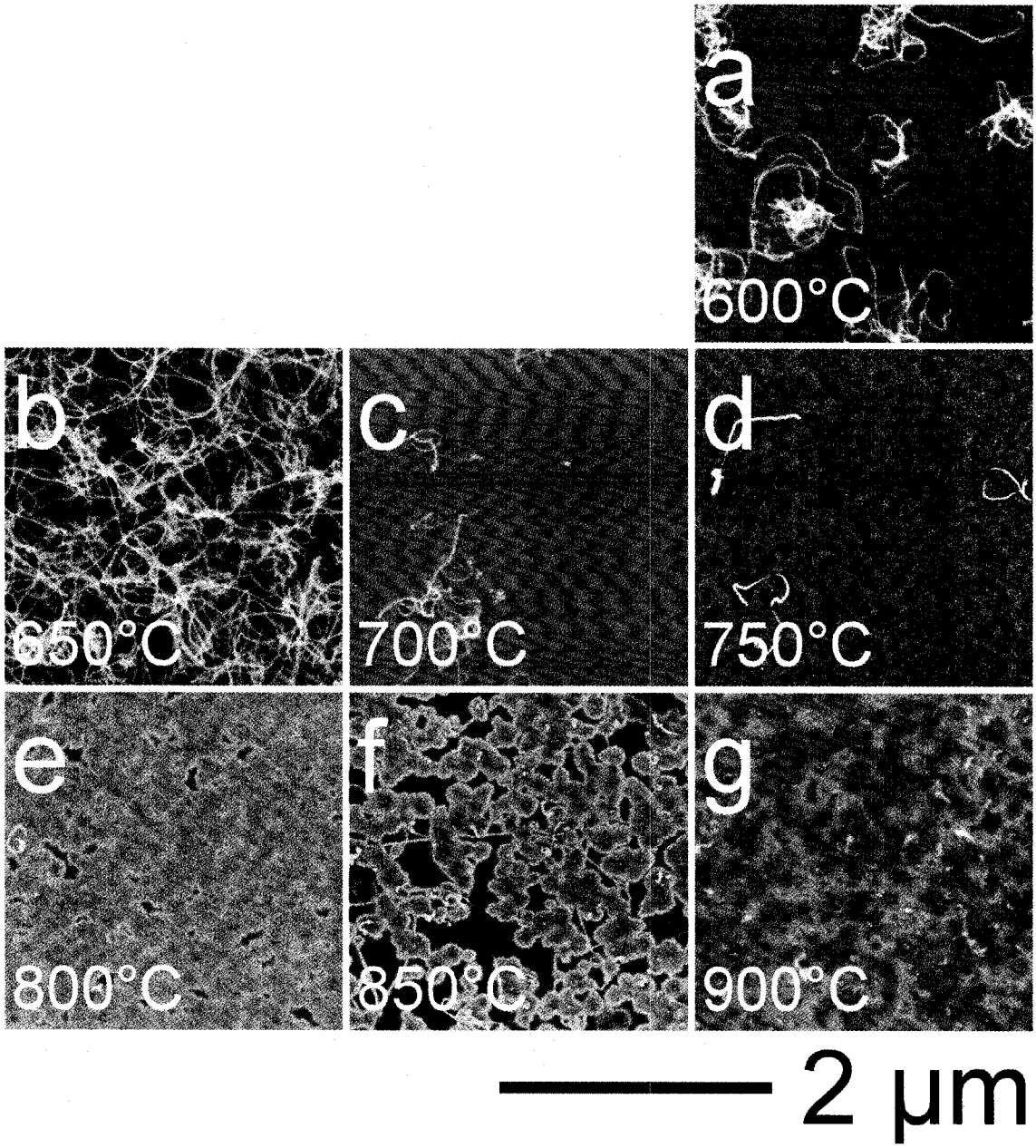

Figure 30 Growth on a 0.02 nm cobalt, 1.0 nm aluminium catalyst taken at 1 kV for various growth temperatures. The growth temperatures were (a) 600°C, (b) 650°C, (c) 700°C, (d) 750°C, (e) 800°C, (f) 850°C and (g) 900°C.

The 1.0 nm/650°C sample contained a thick forest. Growth on 0.1 nm/650°C resulted in the highest yield on this thickness of cobalt. It is difficult to find the substrate through the nanotubes. Nanotubes grown on 0.02 nm/650°C produced the greatest

amount of nanotubes found on this type of catalyst. The yield on 0.02 nm/650°C was less than growth from 0.1 nm/650°C.

Nanotubes produced by growing 1.0 nm/700°C formed of a thick forest. Growth on 0.1 nm/700°C resulted in the formation a thin forest with a large amount of substrate visible. Almost no nanotubes were produced on 0.02 nm/700°C.

Growth on 1.0 nm/750°C produced a thick forest. Growth on 0.1 nm/750°C produced a layer consisting of a large variety of nanotubes. Nanotubes with both large and small diameters were found as well as both short and long nanotubes. The poorest yield of nanotubes found during this set of experiments was found on the 0.02 nm/750°C sample.

The 1.0 nm/800°C growth resulted in a thin layer of nanotubes. Only a few nanotubes were produced of both large and small diameter on the 0.1 nm/800°C growth. The 0.02 nm/800°C growth resulted in the formation of a few nanotubes of varying diameter. This is difficult to see due to charging effects of the substrate.

There are few nanotubes produced by growing on 1.0 nm/850°C. On 0.1 nm/850°C there were even fewer nanotube produced. Growth on 0.02 nm/850°C showed the poorest yield at this temperature. The diameters of all of the nanotubes produced at 850°C vary from thick to thin. The thinner nanotubes are generally much longer than the thicker ones.

Samples grown at 900°C also produced very few nanotubes. The highest yield was found on the 1.0 nm/900°C and the yield was found to decrease with cobalt thickness. A variety of nanotube diameters were found at 900°C similar to 850°C.

7.2 Raman spectroscopy

Raman spectra for these samples with a cobalt catalyst were taken using the same technique detailed in section 4.3. The variation in the concentration of RBMs for the different thicknesses of cobalt can be seen in figure 31.

Comparing figures 28 though 31, the effect of temperature and cobalt thickness can be found. From figure 31 it appears as though the density of radial breathing modes or SWNT is roughly a constant with respect to cobalt thickness at a high growth temperature (850-900°C). Examination of the SEM images of samples grown at these temperatures (f and g of figures 28-30) reveal SWNT candidates. This however is especially difficult to observe on figure 30g due to large surface charging effects. At 800°C the highest concentration of radial breathing modes was found on the 1.0 nm cobalt 1.0 nm aluminium catalyst (figure 31 a IV). The concentration of SWNT then drops off very quickly as the thickness of the cobalt layer decreases. There are very few RBMs on 0.1 nm/800°C and 0.2 nm/800°C (figure 31 b IV, and c IV). This is accounted for by the observation that there are very few nanotubes present on these samples (figures 29e and 30e). Samples grown at 750°C and below also show a decrease in RBM concentration with thinner layers of cobalt. This decrease in RBM concentration is also thought to be caused by the reduction in total nanotube yield on the thinner catalysts.

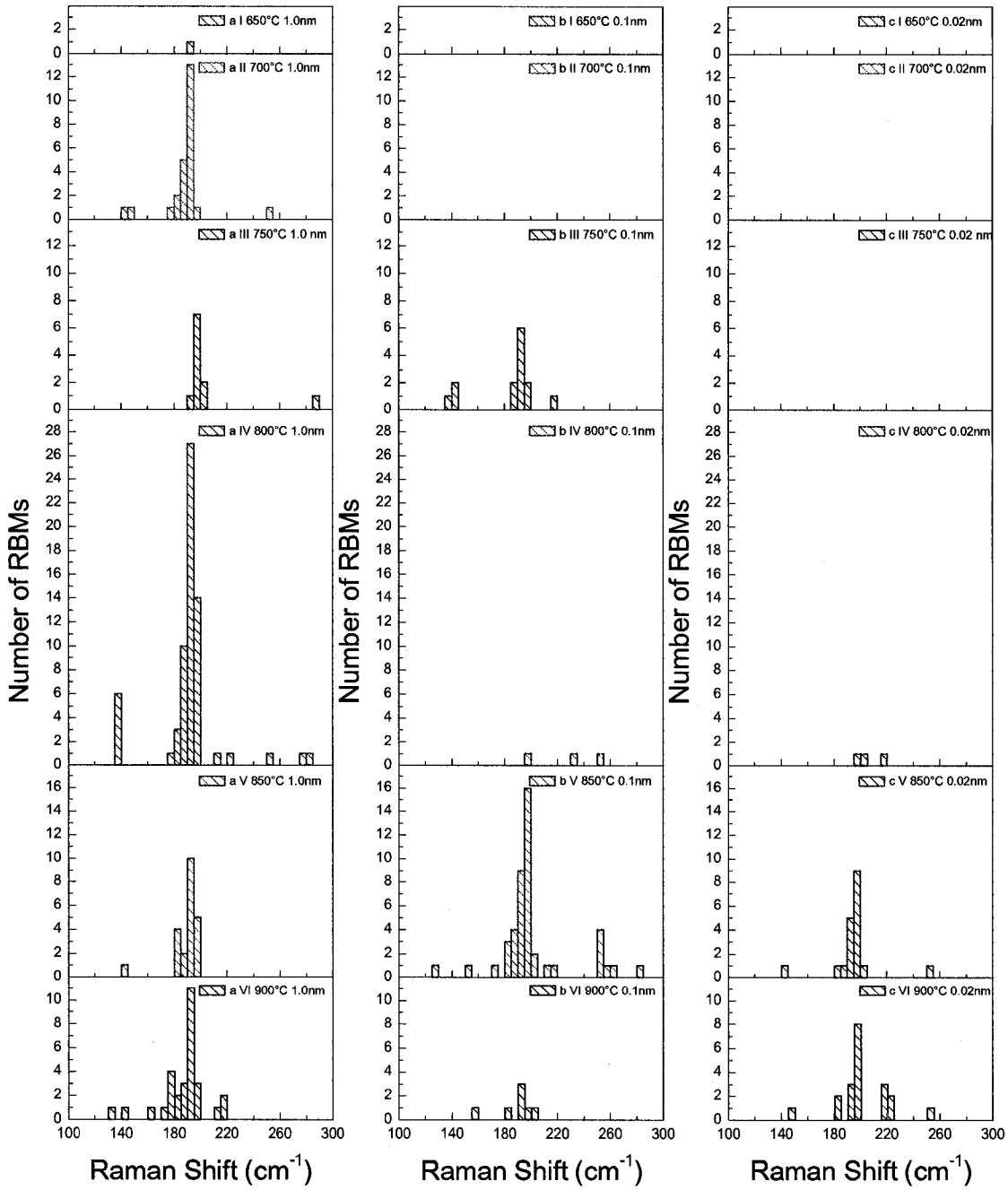

Figure 31 Variation in radial breathing mode concentration with temperature and catalyst thickness. These histograms were generated similarly to the ones in figure 20. All of the samples had a catalyst with a base layer of 1.0 nm aluminium. A cobalt layer with thickness of (a) 1.0 nm, (b) 0.1 nm and (c) 0.02 nm was deposited over the aluminium. The growth temperatures of the samples were (I) 650°C, (II) 700°C, (III) 750°C, (IV) 800°C, (V) 850°C and (VI) 900°C.

7.3 Discussion

In summary, the cobalt thickness appears to have little effect on the growth of nanotubes at high temperatures (850-900°C). Growth at these high temperatures produces a combination of both SWNT and MWNT.

At lower temperatures (600-650°C), growth on a catalyst consisting of 1.0 nm of cobalt and 1.0 nm of aluminium is very good at producing a tall MWNT forest. The nanotube concentration decreases with reductions in the cobalt catalyst thickness.

Growth in between these two sets of temperatures on 0.02 nm/750°C produced very few nanotubes. The nanotube yield was higher at growth temperatures above and below 750°C. This suggests that there is a high temperature small nanoparticle growth mode and a low temperature large nanoparticle or thin film growth mode. Neither of these modes is efficient at 750°C on 0.02 nm of cobalt. Further discussion of this point is deferred to section 10 on page 64.

8 Gas flow dynamics

8.1 Flow rate

Experimentation was performed using a variety of gas flow rates during growth. Some variations in nanotube growth at low temperatures (600-700°C) are thought to be an effect of gas flow rate. A typical forest grown at a temperature of 700°C and with a gas flow rate of 0.6 L/min is shown in figure 32a. A sample grown at the same temperature but a higher gas flow rates (2.3 L/min) was noticed to have sections of nanotube forest which had fallen over in a particular direction. An image of this forest is shown in figure 32b. At high growth temperatures, little variation was noticed when growing at high flow rates.

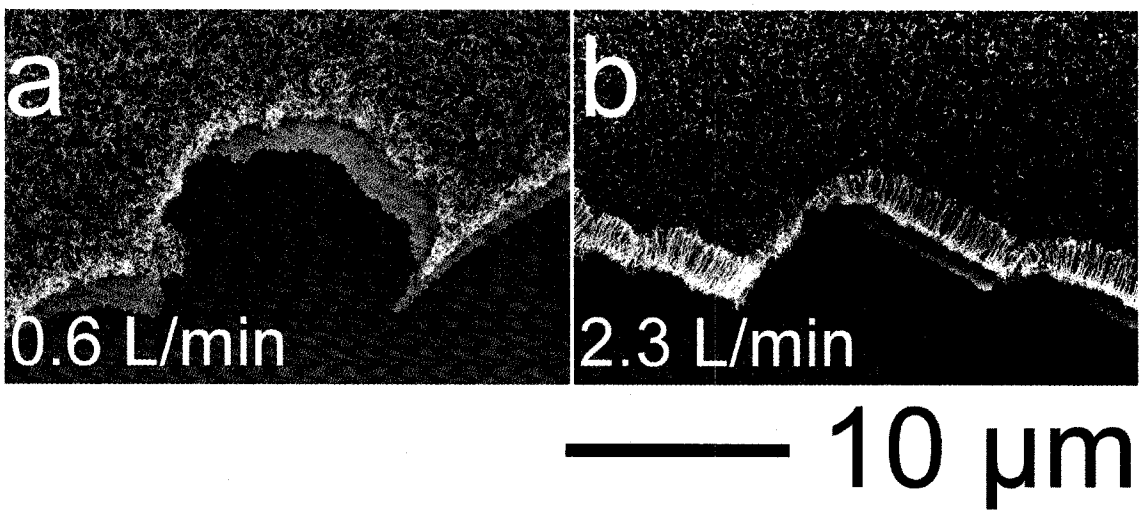

Figure 32 Comparison of gas flow rates during low temperature (700°C) growth. The forest in (a) is vertically aligned and the length of the nanotubes cannot be seen in plan view. The forest in (b) has a tilt in a particular direction possibly due to the gas blowing it over. At certain edges of the catalyst, the length of the nanotubes can be seen.

8.2 Ethanol concentration (dilution)

Experiments were conducted examining how the ethanol concentration during growth affects the nanotubes produced. A 2% hydrogen balance argon mixture was sent through an ethanol bubbler at a variety of different flow rates. The ethanol, hydrogen and argon mixture was then diluted with the hydrogen argon mix to bring the total flow rate up to 0.58 L/min. The only difference between this and previous growth recipes is the amount of ethanol in the gas entering the reactor. The amount of hydrogen and argon entering the reactor is the same as before. The specific recipe for producing these samples is detailed in the appendix section B.4. The results from these experiments at a growth temperature of 850°C are indicated below.

A sample was grown (figure 33 and 34a) with a very high ethanol concentration inside the reactor. Some liquid ethanol was added to the bottom of the reactor before the start of the growth. Some thick nanotubes and a large amount of amorphous likely carbon-based material were found on the sample.

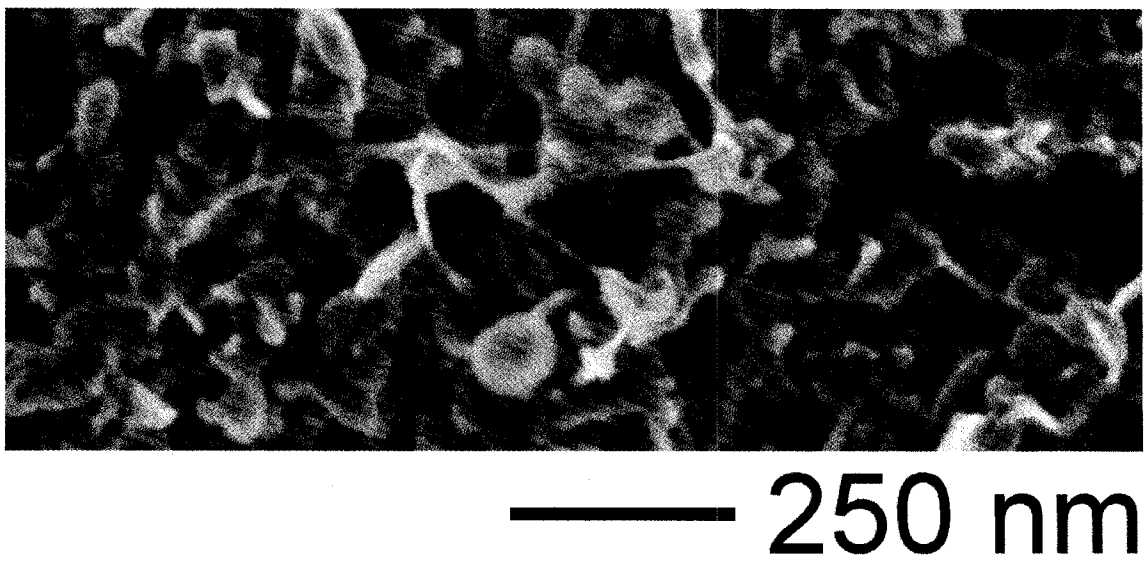

Figure 33 Enlargement of the high ethanol concentration growth (figure 34a).

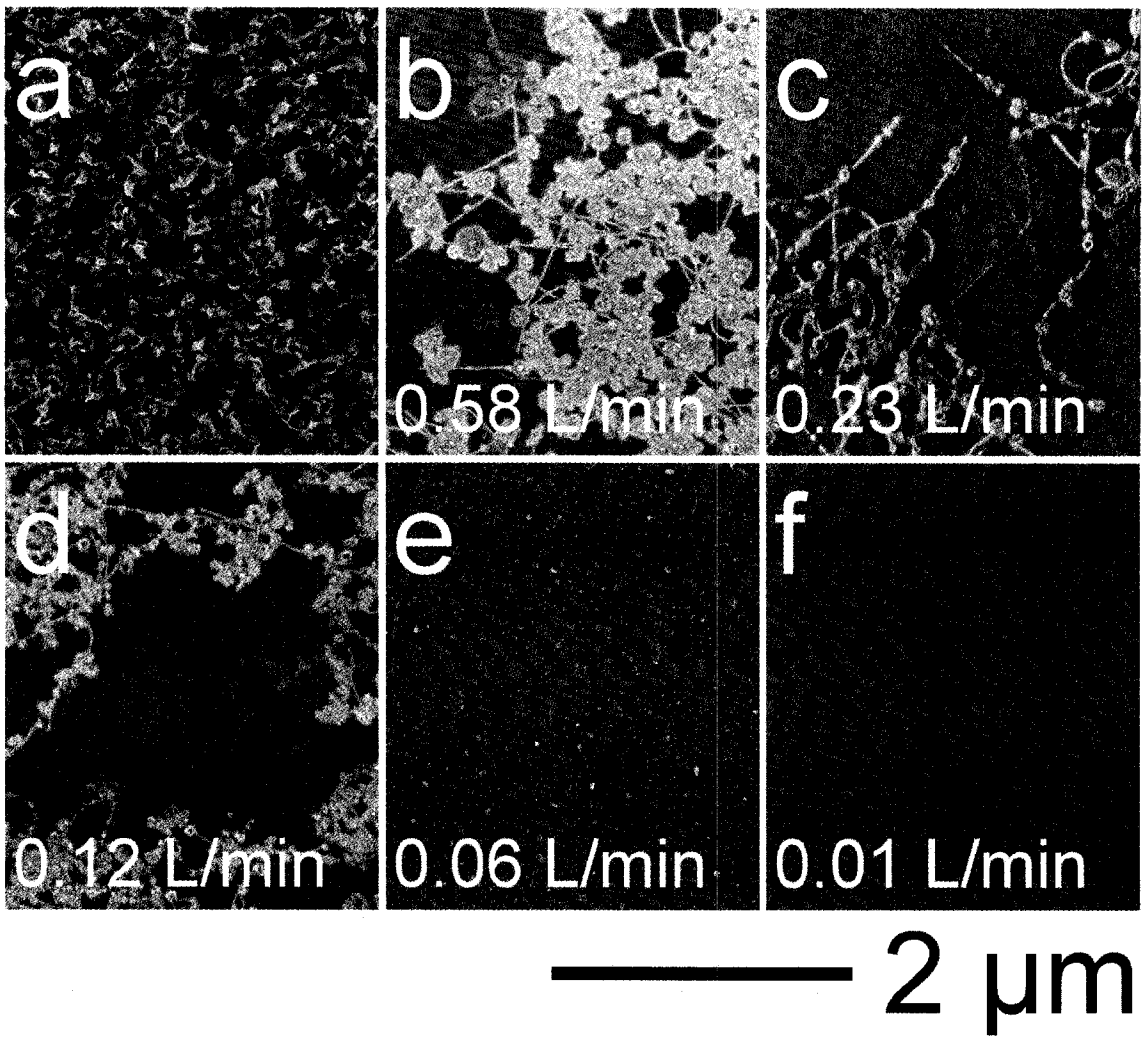

Figure 34 Scanning electron microscope images for various ethanol concentrations. Samples were grown at 850°C for 20 minutes. During growth a mixture of 2% hydrogen balance argon gas was sent through an ethanol bubbler at the flow rate indicated at the bottom of the image. The flow rates were (b) 0.58 L/min, (c) 0.23 L/min, (d) 0.12 L/min, (e) 0.06 L/min and (f) 0.01 L/min. This ethanol, hydrogen and argon mix was diluted with the hydrogen argon gas to bring the total flow rate to 0.58 L/min. This flow then entered the reactor across the sample. In (a) liquid ethanol was added to the bottom of the reactor prior to heating.

Figures 34b-f show how the nanotube concentration varies with ethanol concentration. Figures 34b is a representation of a typical growth at 850°C. Some SWNT candidates are visible on the substrate. No nanotubes were found on the sample grown using an ethanol bubbler flow rate of 0.01 L/min (figure 34f). Samples grown between these bounds had nanotube concentrations relative to the ethanol concentration.

The general result drawn from this set of experiments is that the yield of nanotubes depends on the concentration of ethanol inside the reactor during growth. A decreased concentration of ethanol during growth results in fewer nanotubes. If the ethanol concentration during growth is greater than some threshold then amorphous deposits are formed on the substrate.

8.3 Gas inlets

The reactor had two different inlets from which gas could enter. One inlet was located near the sample so that once gas entered the reactor, it passed directly across the catalyst (figure 16 inlet A). The other inlet was located roughly 7 cm from the sample and was pointed away from the sample (figure 16 inlet B). Experimentation was performed examining the effects of the different inlets on the sample.

During the initial purge to displace air from the reactor the inlet was not found to have any noticeable effect on the growth of nanotubes. Similarly, the choice of inlet during growth had little effect on the nanotubes produced. The largest inlet effect occurred during the final purge before the sample was cooled. Purging across the sample at a high flow rate 2.8 L/min appeared to move the nanotubes around on the sample. On these samples nanotubes were often found at great distances from the catalyst. This is especially noticeable on forest samples. If the final purge entered the reactor away from sample, the forest tended to be much more ordered and fewer nanotubes were found away from the catalyst. This is shown in figure 35. The area to the right of figure 35b, some of which is not shown, contained very few nanotubes in comparison to the area to the right of figure 35a. The adhesion in between some of the nanotubes and the substrate was not strong enough to keep them in place during the final purge at a high gas flow rate.

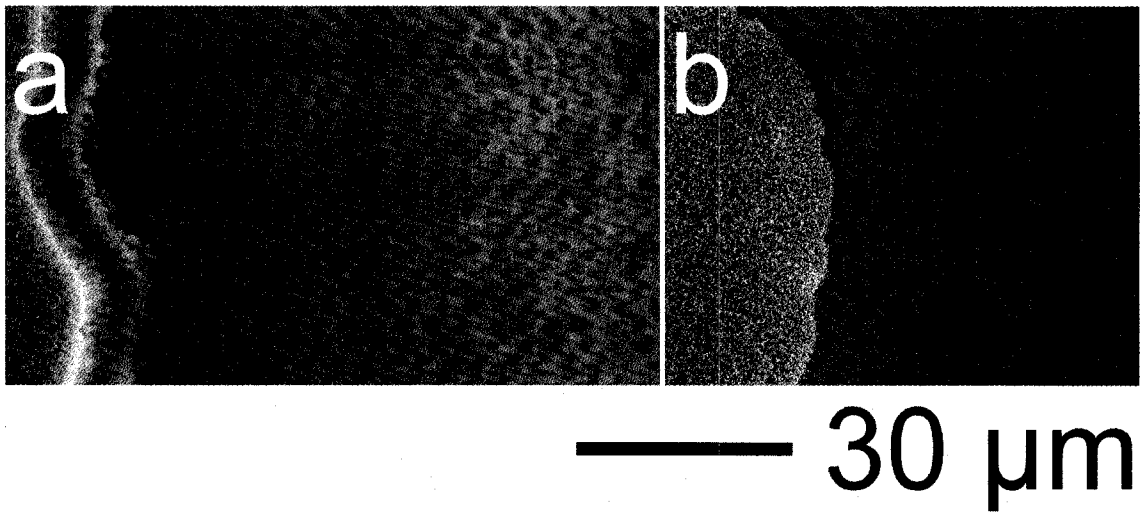

Figure 35 Variations in ethanol purge. High gas flow rates across the sample tended to blow nanotubes around (a) while high flow rates entering the reactor away from the sample did not (b).

9 Growth time

The length of time that the source gas was bubbled through the ethanol bubbler had a large effect on the grown nanotubes. This effect is illustrated by the following figures. Nanotubes were grown very similar to the recipe described in the appendix section B.1. The key differences are that all nanotubes were grown at 650°C and the growth time was varied. A catalyst consisting of 1.0 nm of cobalt and 1.0 nm of aluminium was used for

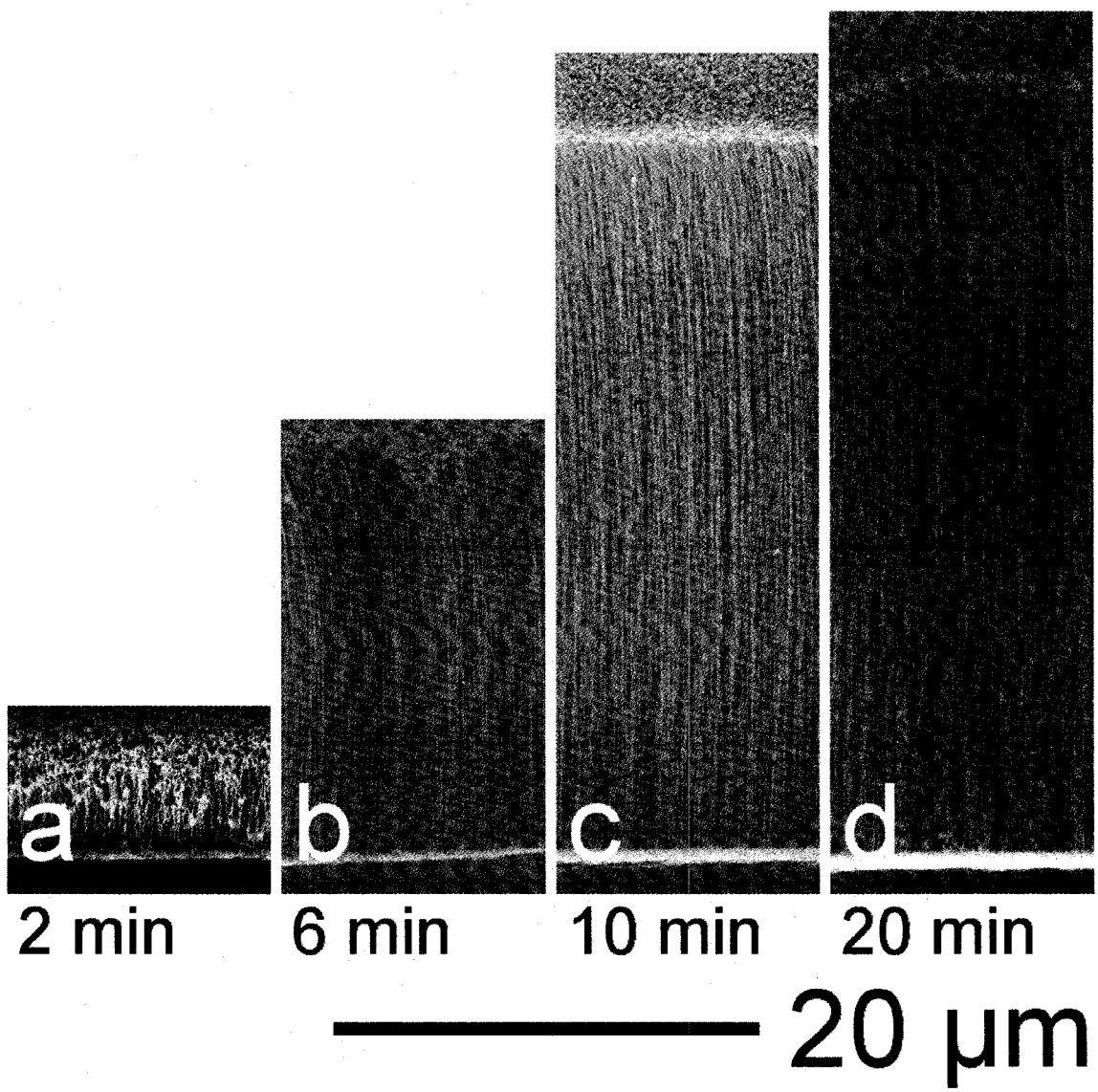

Figure 36 Affect of growth time on nanotube forests. The growth times for (a), (b), (c) and (d) are 2 min, 6 min, 10 min and 20 min respectively.

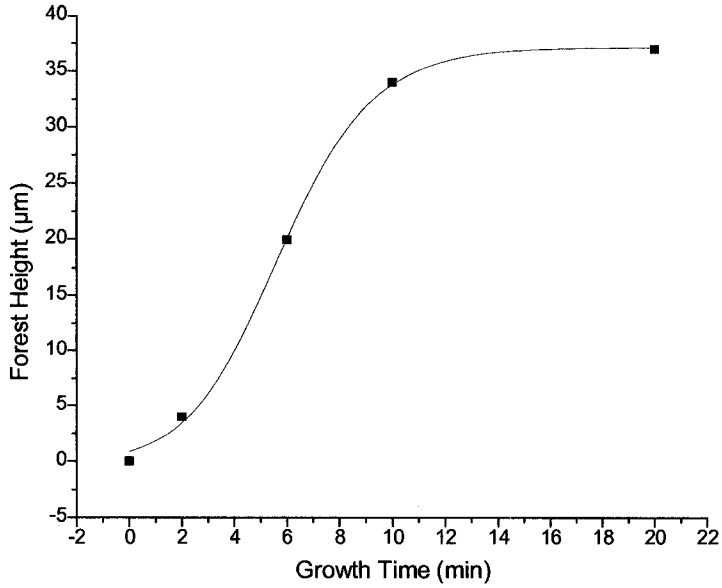

Figure 37 Variation in nanotube forest height with growth time.

this set of experiments. Of all of the catalysts used, this catalyst was found to produce the tallest nanotube forest.

The height of the nanotube forest varied with different growth times. Nanotubes grown for times of 2, 6, 10 and 20 minutes grew to heights of 4, 20, 34 and 37 μm respectively. This is shown in figure 37.

Shortly after ethanol is introduced into the reactor, the growth rate is quick exceeding 2 μm/min. Growth continues at this high growth rate in what could be approximated to be a linear growth region. After 10 minutes however the growth saturates. The growth rate decreases to less than 0.3 μm/min. Other groups have also observed that forest height is limited by this decrease in growth rate with time [78, 79].

10 Growth modes

10.1 Base growth

A sample with an aluminium/iron catalyst was initially grown at 600°C for 20 minutes. This growth produced the vertically aligned multiwalled forest visible in figure 38a. There are some horizontal lines in this image which are artifacts of the imaging conditions. The sample was grown again at 600°C for another 20 minutes. Figure 38b shows the forest after the second growth. There is a horizontal division where some nanotubes from the first growth end and some nanotubes from the second growth begin. Some nanotubes appear to extend the entire height of the forest. Figure 38c is the superposition of a and b together. The only noticeable nanotube growth during the second step occurred between the growth from the first step and the substrate.

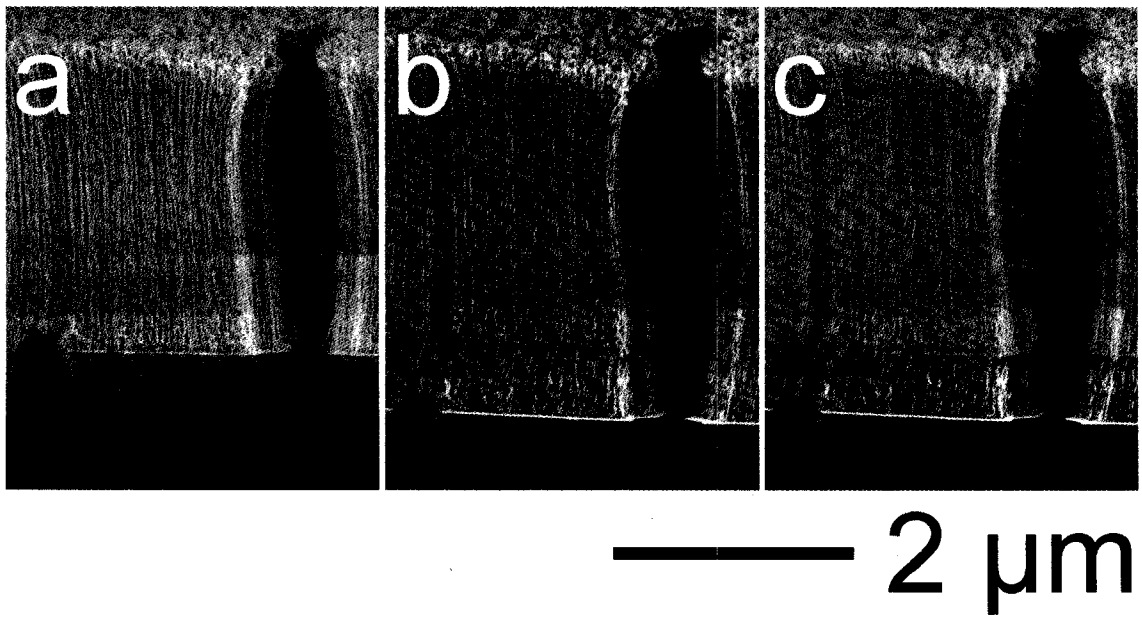

Figure 38 Growth and re-growth of a vertically-aligned nanotube forest in false colour. A sample was grown at 600°C and then examined by scanning electron microscopy (a). It was re-grown and re-examined at the exact same location yielding (b). Image (c) is a superposition of images (a) and (b). The growth from the second step in (c) is blue while the growth from the first step is purple. The horizontal lines which do not divide the growth steps are artifacts resulting from the charging effects of the imaging conditions.

This is strong evidence that nanotube growth at 600°C under these conditions is base growth. Other groups have recently grown nanotubes while varying the carbon isotopes present in the source gas over the course of the growth and agree that base growth is the low temperatures forest producing growth mode [80]. These results lead to the conclusion that the low temperature growth is base growth.

10.2 Tip growth

To contrast, high temperature growth is tip growth. Unless acted upon by some external force (eg AFM tip [81]), once a nanotube makes contact with the substrate it appears to become permanently attached. A nanotube can be examined using PL and then later found in the exact same location on the substrate in SEM. This indicates that there is relatively good adhesion between the nanotube and the substrate. The longest nanotubes observed were all very straight SWNT candidates and grown at high temperatures (figure 39). If these long nanotubes were a result of base growth it is unlikely they would be straight. The adhesion between the nanotube and the substrate would make it difficult for the nanotube to slide large distances (hundreds of micrometers). This resistance would likely introduce large twists and bends over the whole length of the nanotube which are not observed. Some large twists were observed at the end of some nanotubes suggesting that the adhesion between the catalyst and the substrate increased as the growth terminated (figure 39b).

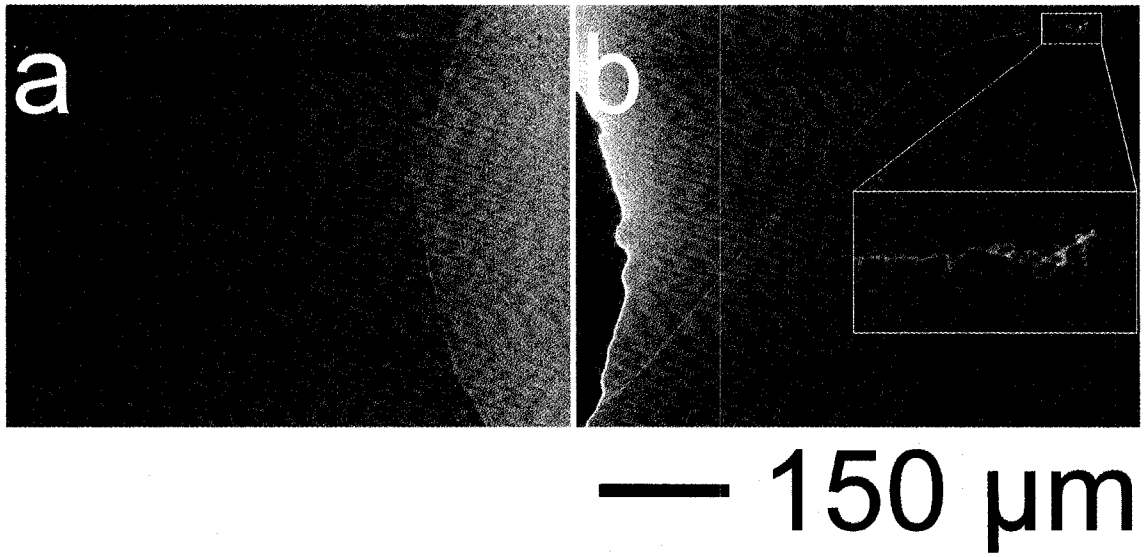

Figure 39 Scanning electron microscope images of long and straight SWNT candidates grown at high temperatures. Both samples were grown at 900°C. The blow up in (b) shows large twists in nanotube direction near one end of a long nanotube.

Nanotubes grown at higher temperatures (figure 40a) had a tendency to grow on the substrate away from the catalyst. It was uncommon to find any nanotubes on the substrate off of the catalyst after a low temperature growth (figure 40b). This is further evidence that high temperature growth results tip growth and a moving catalyst.

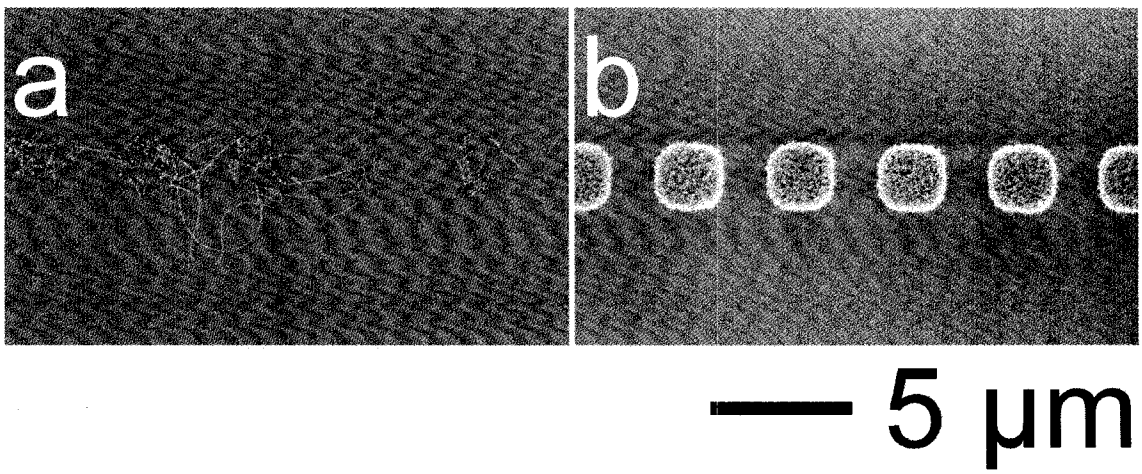

Figure 40 Low and high temperature growth. The only difference between these two growths is the growth temperature. The nanotubes in (a) were grown at 850°C and the nanotubes in (b) were grown at 600°C. All of the nanotube in (b) remain above the catalyst while many of the nanotubes in (a) grew away from the catalyst.

11 Suspension techniques

11.1 Two temperature growth on unpatterned substrates

Combining low and high temperature growth regimes provided a simple means to produce many laterally suspended SWNTs. A shadow mask sample with large iron/aluminium catalyst islands (millimetres in diameter) was grown initially at 600°C for approximately 15 seconds. This initial growth produced a layer of thick MWNTs, too short and sparse to become vertically aligned. The ethanol was purged out and the sample temperature increased to 850°C, after which ethanol was reintroduced for 20 minutes. The second growth sequence caused thin nanotubes to grow over the layer of MWNTs. The specific details of the growth procedure are given in the appendix section B.5.

SEM images of the results are shown in figures 41 and 42. Some of the thick, twisted MWNTs readily seen are standing up forming pillars (figure 41) often extending

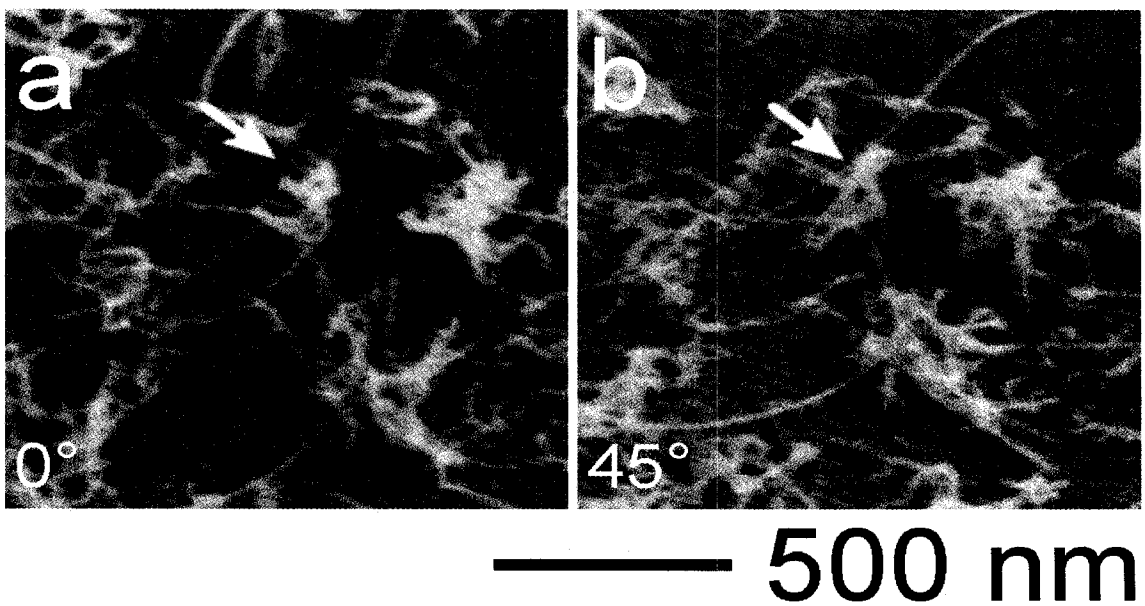

Figure 41 Inclined shadowmask suspension technique. In plan view (a) the clump of multiwalled nanotubes indicated by the arrow appears to be short (~200 nm long). Examining the same location at a 45° tilt (arrow in b) reveals the clump is really longer nanotubes (~400 nm) standing up.

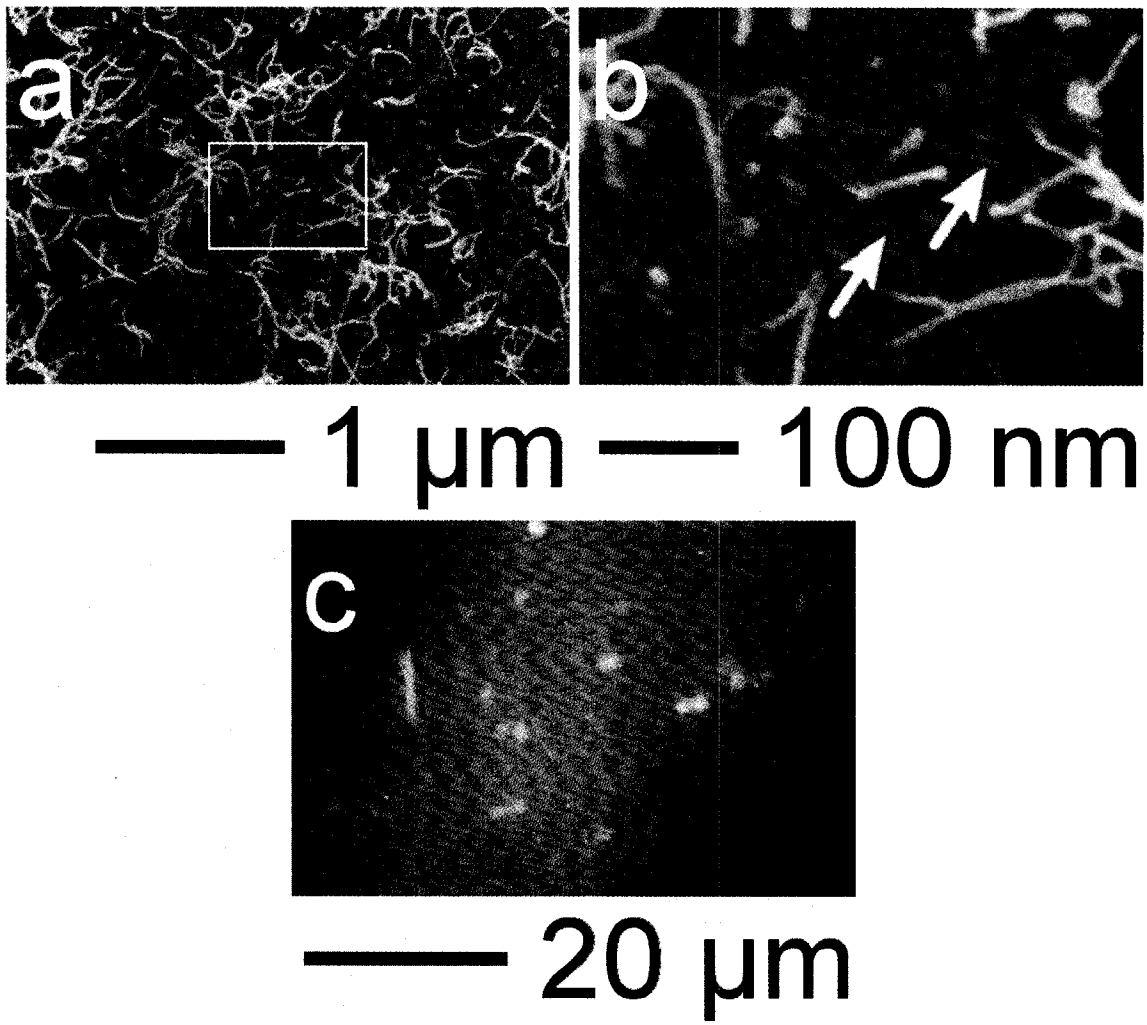

Figure 42 Shadowmask suspension technique [27]. Thin nanotubes, likely single walled (see arrows), are suspended from thicker multi-walled nanotubes. Scanning electron microscope images at 1 kV with (a) low magnification with the box indicating the area imaged in (b) high magnification. Plan view photoluminescence image (c) is from a different area of the same sample. White indicates strong luminescence.

up to a few hundred nanometres above the substrate. These pillars support the thin laterally suspended nanotubes highlighted with arrows. We also used PL imaging to investigate these samples (figure 42c). Different areas were examined with PL and SEM as this sample did not have an indexing system which would allow for us to return to a specific site. The observation of strong PL is additional evidence that many of these thin nanotubes are freely suspended SWNTs.

11.2 Two-temperature growth on patterned substrates

A more organized, webbed network of large numbers of laterally suspended SWNTs was produced with a single photolithographic step. In a photolithography and liftoff process, the catalyst was patterned into roughly circular catalyst dots with a 2 μm diameter and a 4 μm center-to-center spacing.

The CVD process was basically the same as above, but with a longer low temperature growth step to produce a dense forest. The sample was preheated in air, and then reduced in 2% hydrogen, balance argon at 600°C for 10 minutes. Ethanol was then admitted for 20 minutes. This initial growth produced pillars of vertically aligned nanotubes. Ethanol was purged out of the reactor and the sample was heated to 850°C. After another 10 minute hold, ethanol was introduced for another 20 minutes. This second growth resulted in the formation of SWNTs. Many of these SWNTs grew over the forest pillars and connected adjacent MWNT pillars.

This type of result is shown in figure 43. Figure 43a shows a plan view image of an isolated SWNT, marked with an arrow, suspended between two MWNT pillars, left and right. There are also other suspended nanotubes visible in the picture, as well as some nanotubes which lie on the surface of the silicon dioxide. Figure 4b shows the exact same pillar pair seen in side view (85°). The vertical alignment and sharp edges of the MWNT "shrubs" are clear. Finally, figure 43c shows a PL image of the same area. As SEM imaging causes damage which eliminates the PL signal (see section 2.1.3), PL images were taken first. Note that the magnification of the PL image is much lower than the SEM images. The box outlines the exact area imaged by SEM in figure 43a.

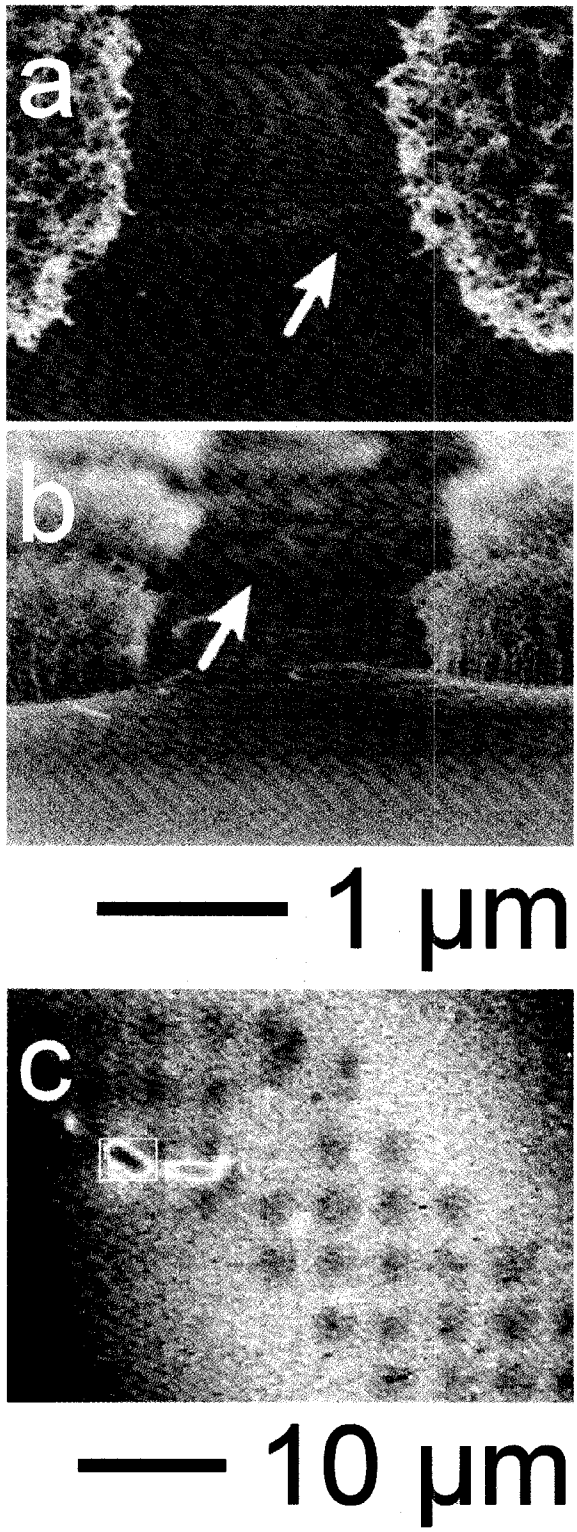

Figure 43 Thin carbon nanotubes supported by vertically aligned nanotube pillars or shrubs [27]. Scanning electron microscope images of the same pair of pillars are shown in (a) plan view at 1 kV, (b) side view (85° tilt angle) at 10 kV. Suspended and surface nanotubes are visible in both images. A photoluminescence image of the same region is shown in (c). The arrows in (a) and (b) indicate the suspended nanotube segment highlighted by the box in (c). Red indicates strong luminescence.

Other suspended nanotube segments visible in the SEM image are not noticeable in the PL image. There are several reasons for this. First, metallic nanotubes and bundles are not expected to emit PL, but are visible in SEM. Second, some nanotubes emit outside our PL detection window (~1.0 μm to 1.6 μm), as their diameter is either too large or too small. Roughly speaking the PL emission wavelength scales linearly with diameter, with a 1 nm diameter nanotube emitting at approximately 1 μm. With reference to tables [82, 83] it can be inferred that this wavelength band corresponds to SWNTs of diameter 0.8 nm to 1.4 nm. A final reason that some of the nanotubes are not visible in the PL image is that those that are excited too far off resonance may absorb too weakly for their PL emission to be detected.

In this work we have developed reliable methods to prepare large numbers of suspended SWNTs. We can say that some fraction are individual isolated SWNTs in our detection window (1.0-1.6 μm) correspond to diameters of ~1-2 nm. We did not control the (n, m) distribution or the fraction of metallic verses non-metallic SWNTs. We have established ways of producing large numbers of suspended SWNTs. Clearly an important future direction is to optimize the distribution of these SWNTs for photonic applications.

11.3 Growth over patterned trenches

A technique commonly used to suspended nanotubes involves nanotube growth over lithography patterned trenches [84]. A 1.0 nm layer of cobalt catalyst was e-beam evaporated on to the substrate. Trenches with widths varying from 3 to 7 μm and a depth of several hundred nanometres were etched in the layer of silicon dioxide. The sample was then grown at a high temperature as to produce thin SWNT. A side view schematic of the sample is shown in figure 44.

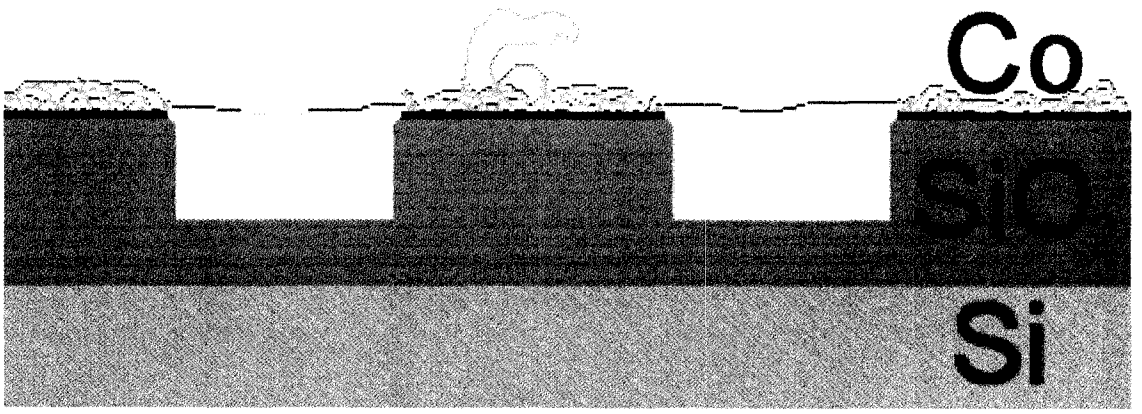

Figure 44 Schematic of the nanotubes (yellow) suspended over lithography patterned trenches.

Figure 45 depicts SEM images of this structure. A large number of thin suspended nanotubes are visible in figure 45a. Surface nanotubes which appear thicker due to substrate charging effects are also visible. Figure 45b is an enlargement of the area indicated by the box in figure 45a. The density of suspended nanotubes as well as bundling events is easily in seen. There are also some carbon deposits around areas where suspended nanotubes intersect.

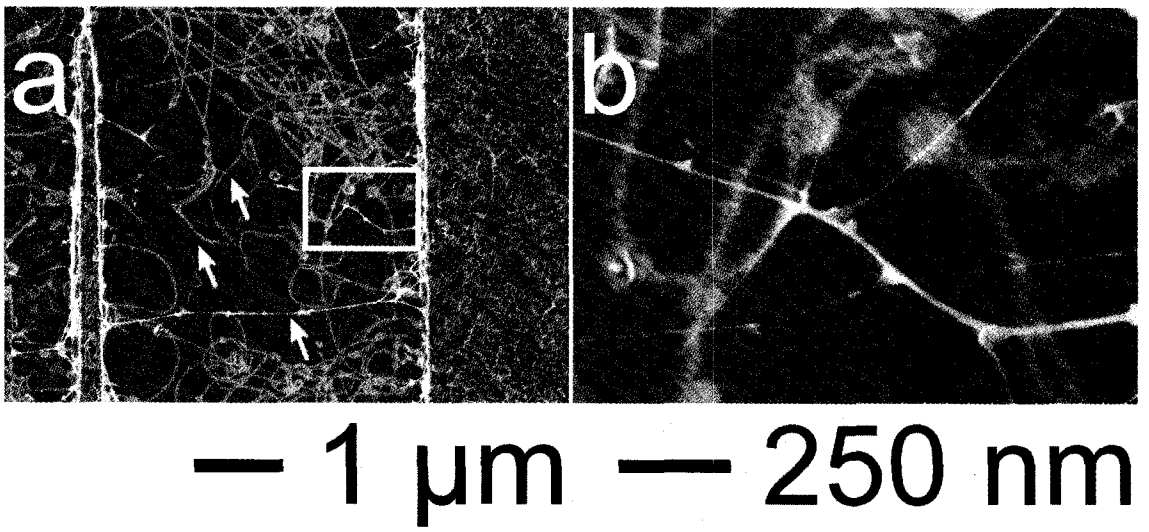

Figure 45 Suspended nanotubes over lithography patterned trenches. The arrows in (a) are over the trench and indicate suspended nanotubes. The box in (a) indicates the area imaged in (b).

12 Conclusions

Two different growth modes are responsible for nanotube growth at different temperatures. The vertically aligned MWNT forest grown at low temperatures (500-700°C) is a result base growth and thin SWNT grown at high temperatures (850-900°C) is tip growth. Base growth occurs from the thin film catalyst. Tip growth is a result of the catalyst breaking up into nanoparticles which under these growth conditions adhere poorly to the substrate.

Different catalysts had different properties which could be used for different applications. A catalyst consisting of 1.0 nm of cobalt on top of 1.0 nm of aluminium produced the tallest vertically aligned forest found (section 9). This catalyst was however poor at producing nanotubes primarily consisting of SWNTs.

A catalyst consisting of only 1.0 nm cobalt produced the greatest number of suspended SWNT on a substrate prepared using photolithography (section 11.3). This catalyst was unable to produce vertically aligned MWNT forests.

A 1.0 nm layer of iron on top of 1.0 nm of aluminium catalyst was well suited for two temperature growths (section 11.2). Other catalysts were found to outperform iron/aluminium at producing only SWNT or only vertically aligned MWNT. No catalyst was found which could produce both SWNTs and vertically aligned MWNT as well as the iron/aluminium combination.

A variety of techniques for producing large numbers of suspended SWNTs were demonstrated. A two temperature CVD growth process can be used to suspend SWNTs over MWNTs. On unpatterned substrates a thin layer of MWNTs can be used to roughen the surface of the substrate allowing for SWNTs to be laterally suspended. On patterned substrates vertically aligned MWNT pillars can be used to elevate sections of SWNTs.

Lithography can be used to prepatterned trenches in the substrate over which SWNTs can be grown. These different approaches have varying complexity and allow for different degrees of control over the suspended nanotubes. The freely suspended SWNTs produced in this work are particularly useful for optical study.

References

[1] Iijima S 1991 *Nature* **354** 56

[2] Dresselhaus M, Dresselhaus G and Avouris P 2001 Carbon Nanotubes: Synthesis, Structure, Properties and Applications. *Springer*

[3] Tans S J, Devoret M H, Dai H, Thess A, Smalley R E, Geerligs L J and Dekker C 1997 *Nature* **386** 474

[4] Bockrath M, Cobden D H, McEuen P L, Chopra N G, Zettl A, Thess A and Smalley R E 1997 *Science* **275** 1922

[5] Tans S J, Verschueren R M and Dekker C, 1997 *Nature* **393** 49

[6] Martel R, Schmidt T, Shea H R, Hertel T and Avourisa P.1998 *Appl. Phys. Lett.* **73** 2447

[7] Collins P G, Zettl A, Bando H, Thess A, Smalley R. E 1997 *Science* **278** 100

[8] Yao Z, Postma H W C, Balents L and Dekker C 1999 *Nature* **402** 273

[9] Fuhrer M S, Nygard J, Shih L, Forero M, Yoon Y G, Mazzoni M S C, Choi H J, Ihm J, Louie S G, Zettl A and McEuen P L 2000 *Science* **288** 494

[10] Saito R, Fujita M, Dresselhaus G and Dresselhaus M S 1992 *Appl. Phys. Lett.* **60** 2204

[11] Zhaon X, Liu Y, Inoue S, Suzuki T, Jones R O and Ando Y 2004 *Phys. Rev. Lett.* **92** 125502

[12] Zheng L X, O'Connell M J, Doorn S K, Liao X Z, Zhao Y H, Akhadov E A, Hoffbauer M A, Roop B J, Jia Q X, Dye R C, Peterson D E, Huang S M, Liu J and Zhu Y T 2004 *Nat. Mater. 3* 673

[13] Bethune D S, Kiang C H, deVries M S, Gorman G, Savoy R, Vazquez J and Beyers R. 1993 *Nature* **363** 605

[14] Journet C, Maser W K, Bernier P, Loiseau A, Delachapelle M L, Lefrant S, Deniard P, Lee R and Fischer J E 1997 *Nature* **388** 756

[15] Thess A, Lee R, Nikolaev P, Dai H, Petit P, Robert J, Xu C, Lee Y H, Kim S G, Rinzler A G, Colbert D T, Scuseria G E, Tomanek D, Fischer J E and Smalley R E 1996 *Science* **273** 483

[16] Kokai F, Takahashi K, Kasuya D, Ichihashi T, Yudasaka M and Iijima S 2000 *Chem. Phys. Letts.* **332** 449

[17] Chen P, Zhang H B, Lin G D, Hong Q and Tsai K R 1997 *Carbon* **35** 1495

[18] Benito A M, Maniette Y, Munoz E and Martinez M T 1998 *Carbon* **36** 681

[19] Finnie P, Bardwell J, Tsandev I, Tomlinson M, Beaulieu M, Fraser J and Lefebvre J 2004 *J. Vac. Sci. Technol. A* **22** 747

[20] Kong J, Cassell A M, and Dai H 1998 *Chem. Phys. Lett.* **292** 567

[21] Chiashi S, Murakami Y, Miyauchi Y and Maruyama S 2004 *Chem. Phys. Lett.* **386** 89

[22] Finnie P, Li-Pook-Than A, Lefebvre J and Austing D G 2006 *Carbon* **44** 3199

[23] Dai H 2001 *Topics in Applied Physics* Springer Verlag Heidelberg **80** 29

[24] Bandow1 S, Asaka S, Saito Y, Rao A M, Grigorian L, Richter E and Eklund P C 1998 *Phys. Rev. Lett.* **80** 3779

[25] Lee Y T, Park J, Choi Y S, Ryu H and Lee H J 2002 *J. Phys. Chem. B* **106** 7614

[26] Unalan H E and Chhowalla M 2005 *Nanotechnology* **16** 2153

[27] Bond J, Lefebvre J, Austing D G, Tay L and Finnie P 2007 *Nanotechnology* **18** 135603

[28] Kong J, Soh H T, Cassell A M, Quate C F and Dai H 1998 *Nature* **395** 878
[29] Li Y M, Kim W, Zhang Y G, Rolandi M, Wang D W and Dai H 2001 *J. Phys. Chem. B* **105** 11424
[30] Hu M H, Murakami Y, Ogura M, Maruyama S and Okubo T 2004 *J. Catal.* **225** 230
[31] Eres G, Kinkhabwala A A, Cui H, Geohegan D B, Puretzky A A and Lowndes D H 2005 *J. Phys. Chem. B* **109** 16684
[32] Cantoro M, Hofmann S, Pisana S, Scardaci V, Parvez A, Ducati C, Ferrari A C, Blackburn A M, Wang K Y and Robertson J 2006 *Nano Lett.* **6** 1107
[33] Takagi D, Homma Y, Hibino H, Suzuki S and Kobayashi Y 2006 *Nano Lett.* **6** 2642
[34] Maruyama S, Kojima R, Miyauchi Y, Chiashi S, Kohno M *Chem. Phys. Lett.* **360** 229
[35] Dai H, Rinzler A G, Nikolaev P, Thess A, Colbert D T and Smalley R E *Chem. Phys. Lett.* **260** 471
[36] Hafner J H, Bronikowski M J, Azamian B R, Nikolaev P, Rinzler A G, Colbert D T, Smith K A and Smalley R E *Chem. Phys. Lett.* **296** 195
[37] Satishkumar B C, Govindaraj A, Sen R and Rao C N R *Chem. Phys. Lett.* **293** 47
[38] Tibbetts G G 1984 *J. Cryst. Growth* **66** 632
[39] Baker R T K 1989 *Carbon* **27** 315
[40] Amelinckx S, Zhang X B, Bernaerts D, Zhang X F,Ivanov V and Nagy J B 1994 *Science* **265** 635
[41] Pulker H K, Perry A J and Berger R 1981 *Surf. Technol.* **14** 25
[42] Ward J W, Wei B Q and Ajayan P M 2006 *Chem. Phys. Lett.* **376** 717
[43] Matthews K D, Lemaitre M G, Kim T, Chen H, Shim M and Zuob J M 2006 *J. Appl. Phys.* **100** 44309
[44] Wei Y Y, Eres G, Merkulov V I and Lowndes D H 2001 *Appl. Phys. Lett.* **78** 1394
[45] Lefebvre J, Homma Y and Finnie P 2003 *Phys. Rev. Lett.* **90** 217401
[46] Lefebvre J, Austing D G, Bond J and Finnie P 2006 *Nano Lett.* **6** 1603
[47] Misewich J A, Martel R, Avouris P, Tsang J C, Heinze S and J. Tersoff 2003 *Science* **300** 783
[48] LeRoy B J, Lemay S G, Kong J and Dekker C 2004 *Nature* **432** 371
[49] Chen J, Perebeinos V, Freitag M, Tsang J, Fu Q, Liu J and Avouris P 2005 *Science* **310** 1171
[50] Kobayashi Y, Yamashita T, Ueno Y, Niwa O, Homma Y and Ogino T 2004 *Chem. Phys. Lett.* **386** 153
[51] Son H, Hori Y, Chou S G, Nezich D, Samsonidze G G, Dresselhaus G, Dresselhaus M S and Barros E B 2004 *Appl. Phys. Lett.* **85** 4744
[52] Zhang Y, Zhang J, Son H, F J and Liu Z 2005 *J. Am. Chem. Soc.* **127** 17156
[53] Cassell A M, Franklin N R, Tombler T W, Chan E M, Han J and Dai H 1999 *J. Am. Chem. Soc.* **121** 7975
[54] Homma Y, Kobayashi Y, Ogino T and Yamashita T 2002 *Appl. Phys. Lett.* **81** 2261
[55] Chikkannanavar S B, Luzzi D E, Paulson S and Johnson A T 2005 *Nano Lett.* **5** 151
[56] Yang B, Marcus M S, Keppel D G, Zhang P P, Li Z W, Larson B J, Savage D E, Simmons J M, Castellini O M, Eriksson M A and Lagally M G 2005 *Appl. Phys. Lett.* **86** 263107
[57] Walters D A, Ericson L M, Casavant M J, Liu J, Colbert D T, Smith K A and Smalley R E 1999 *Appl. Phys. Lett.* **74** 3803

[58] Brintlinger T, Chen Y F, Durkop T, Cobas E and Fuhrer M S 2002 *Appl. Phys. Lett.* **81** 2454
[59] Zhang R Y, Wei Y, Nagahara L A, Amlani I and Tsui R K 2006 *Nanotechnology* **17** 272
[60] Suzuki S, Kanzaki K, Homma Y, and Fukuba S 2004 *Jpn. J. Appl. Phys.* **43** L1118
[61] Yuzvinsky T D, Fennimore A M, Mickelson W, Esquivias C and Zettl A 2005 *Appl. Phys. Lett.* ***86*** 53109
[62] Koops H W P, Weiel R, Kern D P and Baum T H 1988 *J. Vac. Sci. Technol. B* **6** 477
[63] Vigouroux J P, Duraud J P, Le Moel A and Le Gressus C 1985 *J. Appl. Phys.* **57** 5139
[64] Homma Y, Suzuki S, Kobayashi Y and Nagase M 2004 *Appl. Phys. Lett.* **84** 1750
[65] Bachtold A, Fuhrer M. S, Plyasunov S, Forero M, Anderson E H, Zettl A and McEuen P L 2000 *Phys. Rev. Lett.* **84** 6082
[66] Rao A M, Richter E, Bandow S, Chase B, Eklund P C, Williams K A, Fang S, Subbaswamy K R, Menon M, Thess A, Smalley R E, Dresselhaus G and Dresselhaus M S 1997 *Science* **275** 187
[67] Bandow S, Takizawaa M, Hiraharaa K, Yudasakac M and Iijimaa S 2001 *Chem. Phys. Lett.* **337** 48
[68] Dresselhaus M S, Dresselhaus G, Jorio A, Filho A G S and Saito R 2002 *Carbon* **40** 2043
[69] Kaminska K, Lefebvre J, Austing D G and Finnie P 2006 *Phys. Rev. B* **73** 235410
[70] Kataura H, Kumazawa Y, Maniwa Y, Umezu I, Suzuki S, Ohtsuka Y and Achiba Y 1999 *Synth. Met.* **103** 2555
[71] Tsyboulski D A, Bachilo S M and Weisman R B 2005 *Nano Lett.* **5** 975
[72] Hartschuh A, Pedrosa H N, Novotny L and Krauss T D 2003 *Science* **301** 1354
[73] O'Connell M J, Bachilo S M, Huffman C B, Moore V C, Strano M S, Haroz E H, Rialon K L, Boul P J, Noon W H, Kittrell C, Ma J, Hauge R H, Weisman R B and Smalley R E 2002 *Science* **297** 593
[74] Harigaya K 1999 *Phys. Rev. B* **60** 1452
[75] Hertel T, Hagen A, Talalaev V, Arnold K, Hennrich F, Kappes M, Rosenthal S, McBride J, Ulbricht H and Flahaut E 2005 *Nano. Lett.* **5** 511
[76] Okazaki T, Bandow S, Tamura G, Fujita Y, Iakoubovskii K, Kazaoui S, Minami N, Saito T, Suenaga K and Iijima S 2006 *Phys. Rev. B* **74** 153404
[77] Maruyama S, Kojima R, Miyauchi Y, Chiashi S and Kohno M 2002 *Chem. Phys. Lett.* **360** 229
[78] Bower C and Zhou O 2000 *Appl. Phys. Lett.* **77** 2767
[79] Maruyama S, Einarsson E, Murakami Y and Edamura T 2005 *Chem. Phys. Lett.* **403** 320
[80] Khodja H, Pinault M, Mayne-L'Hermite M and Reynaud C 2006 *Nucl. Instr. and Meth. B* **249** 523
[81] Roschier L, Penttila J, Martin M, Hakonen P, Paalanen M, Tapper U, Kauppinen E I, Journet C and Bernier P 1999 *Appl. Phys. Lett.* **75** 728
[82] Bachilo S M, Strano M S, Kittrell C, Hauge R H, Smalley R E and Weisman R B 2002 *Science* **298** 2361
[83] Weisman R B and Bachilo S M 2003 *Nano Lett.* **3** 1235

[84] Franklin N R, Wang Q, Tombler T W, Javey A, Shim M and Dai H 2002 *Appl. Phys. Lett.* **81** 913

Appendix A: Legend

AFM – atomic force microscopy or atomic force microscope
CVD – chemical vapour deposition
CNT – carbon nanotube
DWNT – double walled carbon nanotube
MWNT – multiwalled carbon nanotube
PL – photoluminescence
SEM – scanning electron microscopy or scanning electron microscope
SWNT – single walled carbon nanotube

Appendix B: Growth recipes

B.1 Growth temperature

This growth recipe is the basic recipe from which all of the other recipes were derived from.

- remove the heater from the reactor to expose the reactor to air
- clip the cleaved sample to the heater
- insert the heater with the sample inside the reactor and seal the reactor
- heat sample to 300°C as measured by the thermocouple in the air inside the reactor for 10 minutes
- turn off the heat and allow the sample to cool
- after the sample cools below 100°C, measured by the thermocouple, start a flow of argon at 2.8 L/min
- after 5 minutes of argon flow, switch the purge gas to 2% hydrogen/argon also at 2.8 L/min
- after 5 minutes of 2% hydrogen/argon flow reduce the flow rate to 0.6 L/min and turn on the heater
- heat the sample to the growth temperature as measured using the Pyrometer (the growth temperatures are indicated in figure 18)
- wait 10 minutes after the sample has reached the growth temperature to soak in hydrogen
- after the soak in hydrogen, reroute the inlet gas through the bubbler
- bubble ethanol for a growth time of 20 minutes
- divert gas flow to bypass the bubbler and increase flow rate to 2.8 L/min for 5 minutes to purge reactor
- turn off heat
- after the sample cools below 100°C turn off 2% hydrogen/argon flow

B.2 Soak in hydrogen

This growth recipe involves different temperatures in the soak in hydrogen and growth phases.

- remove the heater from the reactor to expose the reactor to air
- clip the cleaved sample to the heater
- insert the heater with the sample inside the reactor and seal the reactor
- heat sample to 300°C as measured by the thermocouple in the air inside the reactor for 10 minutes
- turn off the heat and allow the sample to cool
- after the sample cools below 100°C, measured by the thermocouple, start a flow of argon at 2.8 L/min

- after 5 minutes of argon flow, switch the purge gas to 2% hydrogen/argon also at 2.8 L/min
- after 5 minutes of 2% hydrogen/argon flow reduce the flow rate to 0.6 L/min and turn on the heater
- heat the sample to the **soak in hydrogen** temperature as measured using the Pyrometer (either 850°C or 900°C)
- wait 10 minutes after the sample has reached the growth temperature to soak in hydrogen
- **reduce the sample temperature to the growth temperature as quickly as possible (growth temperatures are indicated in figures 24 and 25)**
- **after the sample reaches the growth temperature**, reroute the inlet gas through the bubbler
- bubble ethanol for a growth time of 20 minutes
- divert gas flow to bypass the bubbler and increase flow rate to 2.8 L/min for 5 minutes to purge reactor
- turn off heat
- after the sample cools below 100°C turn off 2% hydrogen/argon flow

B.3 Nanoparticles

Samples were preheated in air at 300°C. The samples were then heated in hydrogen/argon to typical growth temperatures for 10 minutes. Prior to the introduction of ethanol into the reactor, the heater was turned off and the sample was allowed to cool as quickly as possible to room temperature

- remove the heater from the reactor to expose the reactor to air
- clip the cleaved sample to the heater
- insert the heater with the sample inside the reactor and seal the reactor
- heat sample to 300°C as measured by the thermocouple in the air inside the reactor for 10 minutes
- turn off the heat and allow the sample to cool
- after the sample cools below 100°C, measured by the thermocouple, start a flow of argon at 2.8 L/min
- after 5 minutes of argon flow, switch the purge gas to 2% hydrogen/argon also at 2.8 L/min
- after 5 minutes of 2% hydrogen/argon flow reduce the flow rate to 0.6 L/min and turn on the heater
- heat the sample to the growth temperature as measured using the Pyrometer (the growth temperatures are indicated in figure 26)
- **wait 10 minutes after the sample has reached the growth temperature to soak in hydrogen**
- **turn off heat**
- after the sample cools below 100°C turn off 2% hydrogen/argon flow

B.4 Ethanol concentration

The concentration of ethanol inside the reactor during growth was varied. This was done by diluting the gas after it passed through the bubbler but before it entered the reactor.

- remove the heater from the reactor to expose the reactor to air
- clip the cleaved sample to the heater
- insert the heater with the sample inside the reactor and seal the reactor
- heat sample to 300°C as measured by the thermocouple in the air inside the reactor for 10 minutes
- turn off the heat and allow the sample to cool
- after the sample cools below 100°C, measured by the thermocouple, start a flow of argon at 2.8 L/min
- after 5 minutes of argon flow, switch the purge gas to 2% hydrogen/argon also at 2.8 L/min
- after 5 minutes of 2% hydrogen/argon flow reduce the flow rate to 0.6 L/min and turn on the heater
- heat the sample to the growth temperature **of 850°C** as measured using the Pyrometer
- wait 10 minutes after the sample has reached the growth temperature to soak in hydrogen
- after the soak in hydrogen, reroute **some** the inlet gas through the bubbler **(the gas flow rates through the bubbler are indicated on figure 34, the total flow entering the reactor was 0.58 L/min)**
- bubble ethanol for a growth time of 20 minutes
- divert gas flow to bypass the bubbler and increase flow rate to 2.8 L/min for 5 minutes to purge reactor
- turn off heat
- after the sample cools below 100°C turn off 2% hydrogen/argon flow

B.5 Two temperature growth

A two temperature growth involves soaking in hydrogen and then growing at one temperature and then soaking in hydrogen and growing at a different temperature. The most ideal catalyst examined for this type of growth is 1.0 nm of iron on top of 1.0 nm of aluminium.

- remove the heater from the reactor to expose the reactor to air
- clip the cleaved sample to the heater
- insert the heater with the sample inside the reactor and seal the reactor
- heat sample to 300°C as measured by the thermocouple in the air inside the reactor for 10 minutes
- turn off the heat and allow the sample to cool
- after the sample cools below 100°C, measured by the thermocouple, start a flow of argon at 2.8 L/min
- after 5 minutes of argon flow, switch the purge gas to 2% hydrogen/argon also at 2.8 L/min

- after 5 minutes of 2% hydrogen/argon flow reduce the flow rate to 0.6 L/min and turn on the heater
- heat the sample to the **1st** growth temperature **of 600°C** as measured using the Pyrometer
- wait 10 minutes after the sample has reached the growth temperature to soak in hydrogen
- after the soak in hydrogen, reroute the inlet gas through the bubbler
- bubble ethanol for **the 1st growth time**
- **divert gas flow to bypass the bubbler and heat the sample to the 2st growth temperature of 850°C as measured using the Pyrometer**
- **wait 10 minutes after the sample has reached the growth temperature to soak in hydrogen**
- **after the soak in hydrogen, reroute the inlet gas through the bubbler**
- **bubble ethanol for the 2nd growth time**
- divert gas flow to bypass the bubbler and increase flow rate to 2.8 L/min for 5 minutes to purge reactor
- turn off heat
- after the sample cools below 100°C turn off 2% hydrogen/argon flow